NeuroImage 83 (2013) 174–188

Contents lists available at ScienceDirect

NeuroImage

journal homepage: www.elsevier.com/locate/ynimg

Tackling the multifunctional nature of Broca's region meta-analytically: Co-activation-based parcellation of area 44

Mareike Clos [a,*], Katrin Amunts [a,b,c,d], Angela R. Laird [e], Peter T. Fox [f,h], Simon B. Eickhoff [a,g]

[a] Institute of Neuroscience and Medicine (INM-1), Research Centre Jülich, Germany
[b] JARA-BRAIN, Jülich-Aachen Research Alliance, Germany
[c] Department of Psychiatry, Psychotherapy, and Psychosomatics, RWTH Aachen, Germany
[d] C. and O. Vogt Institute for Brain Research, Heinrich Heine University, Düsseldorf, Germany
[e] Department of Physics, Florida International University, Miami, FL, USA
[f] Research Imaging Institute, University of Texas Health Science Center at San Antonio, TX, USA
[g] Institute of Clinical Neuroscience and Medical Psychology, Heinrich Heine University, Düsseldorf, Germany
[h] South Texas Administration Medical Center, San Antonio, TX, USA

ARTICLE INFO

Article history:
Accepted 11 June 2013
Available online 19 June 2013

Keywords:
Activation likelihood estimation
Functional connectivity
K-means clustering
Language
Meta-analytic connectivity modeling

ABSTRACT

Cytoarchitectonic area 44 of Broca's region in the left inferior frontal gyrus is known to be involved in several functional domains including language, action and music processing. We investigated whether this functional heterogeneity is reflected in distinct modules within cytoarchitectonically defined left area 44 using meta-analytic connectivity-based parcellation (CBP). This method relies on identifying the whole-brain co-activation pattern for each area 44 voxel across a wide range of functional neuroimaging experiments and subsequently grouping the voxels into distinct clusters based on the similarity of their co-activation patterns. This CBP analysis revealed that five separate clusters exist within left area 44. A post-hoc functional characterization and functional connectivity analysis of these five clusters was then performed. The two posterior clusters were primarily associated with action processes, in particular with phonology and overt speech (posterior-dorsal cluster) and with rhythmic sequencing (posterior-ventral cluster). The three anterior clusters were primarily associated with language and cognition, in particular with working memory (anterior-dorsal cluster), with detection of meaning (anterior-ventral cluster) and with task switching/cognitive control (inferior frontal junction cluster). These five clusters furthermore showed specific and distinct connectivity patterns. The results demonstrate that left area 44 is heterogeneous, thus supporting anatomical data on the molecular architecture of this region, and provide a basis for more specific interpretations of activations localized in area 44.

Introduction

Area 44, as mapped cytoarchitectonically by Brodmann (1909), corresponds to the posterior part of Broca's region on the inferior frontal gyrus. More recently, the borders of this area have been redefined cytoarchitechtonically using observer-independent techniques in a series of histological sections of 10 postmortem brains (Amunts et al., 1999). Being part of Broca's speech region, left area 44 is known to be involved in both language production and comprehension although its exact contribution to language comprehension is still a matter of debate (Friederici, 2011; Hagoort, 2005). In addition to this core function, however, area 44 also plays a role in several non-language-related functions such as working memory (Buchsbaum et al., 2005; Kaan and Swaab, 2002; Rogalsky and Hickok, 2011; Smith and Jonides, 1999), execution and perception of action (as part of the mirror-neuron system; Clerget et al., 2009; Fazio et al., 2009; Heiser et al., 2003; Iacoboni et al., 1999; Rizzolatti and Craighero, 2004) and the processing of music (Koelsch, 2011; Koelsch et al., 2002; Maess et al., 2001; Platel et al., 1997). This raises the question whether this cytoarchitectonic area may indeed be regarded as a single, homogeneous functional module. Supporting the view of a structural heterogeneity within area 44, a recent postmortem, receptor-based parcellation of Broca's region indicated the presence of distinct subareas within this cytoarchitectonic region (Amunts et al., 2010). In this study left area 44 was divided into an anterior-dorsal area 44d and a posterior-ventral area 44v using multi-receptor mapping. Since transmitter receptors are key molecules for neurotransmission, it can be assumed that this heterogeneity at the molecular level corresponds to a similar differentiation at the level of function and connectivity. Evidence of such a differentiation may be achieved with connectivity-based parcellation (CBP) of functional imaging data. The rationale behind CBP is that functionally homogenous subregions show very similar connectivity patterns, which at the same time are clearly distinguished from that of other subregions. Connectivity measures employed in CBP approaches include diffusion-tensor imaging

* Corresponding author at: Forschungzentrum Jülich, INM-1, 52425 Jülich, Germany. Fax: +49 2461 61 2990.
E-mail address: m.clos@fz-juelich.de (M. Clos).

1053-8119/$ – see front matter © 2013 Elsevier Inc. All rights reserved.
http://dx.doi.org/10.1016/j.neuroimage.2013.06.041

(Johansen-Berg et al., 2004), resting state functional connectivity (Zhang and Li, 2012), and meta-analytic connectivity modeling (Cauda et al., 2012; Eickhoff et al., 2011). Previous DTI parcellations targeting Broca's region have demonstrated that areas 44 and 45 can be distinguished from each other based on their connectivity patterns (Anwander et al., 2007; Ford et al., 2010; Klein et al., 2007). However, as these studies focused mainly on the inter-area differences, no intra-area subdivisions have been identified.

In order to investigate whether functionally distinct subregions exist within the left area 44, we used a meta-analytic connectivity modeling (MACM) based parcellation (Bzdok et al., 2012a; Cieslik et al., 2012). This approach makes use of the BrainMap database (Fox and Lancaster, 2002; Laird et al., 2005, 2009a, 2011) to identify the whole-brain co-activation pattern for each voxel within area 44 across a wide range of neuroimaging experiments. The resulting individual co-activation profiles are then compared between voxels to identify clusters of voxels showing very similar co-activation patterns. Furthermore, a follow-up MACM analysis on the derived clusters was performed to reveal the overall and specific co-activation networks of these clusters. Finally, the function of the clusters in terms of behavioral domains and paradigm classes was determined from the associated BrainMap meta-data. Note that the parcellation was only based on the whole-brain co-activation pattern of the individual voxels and that the decision regarding the optimal parcellation solution was based on external stability criteria. Subsequently, only the most stable parcellation solution was functionally characterized post-hoc based on specific connectivity and BrainMap meta-data of the individual clusters (for an overview of the method see Fig. 1).

Material and methods

Meta-analytic connectivity mapping

The volume-of-interest (VOI) for the current CBP analysis was provided by representation of left area 44 in the maximum probability map (MPM) in the SPM Anatomy Toolbox (Eickhoff et al., 2005, 2006a). This MPM was derived from the cytoarchitectonic mapping of 10 postmortem human brains (Amunts et al., 1999) registered to 3D MNI space (Montreal Neurological Institute; Amunts et al., 2004; Evans et al., 2012) and specifies the likelihood that a particular cortical area is localized at each brain voxel. This whole-brain MPM thus provides a continuous, non-overlapping representation of the microanatomically defined area 44 and allows the user to define a VOI that includes only those voxels which are more likely to represent area 44 than any other cytoarchitectonic area. It should be noted that normalization into standard space (which is slightly bigger than an average brain) as well as representation of microscopical structures in $2 \times 2 \times 2$ mm^3 voxel space may result in a rather liberal definition of area 44 as compared to the stereological volume measured in postmortem data at micrometer histological resolution. Nevertheless, the MPM-based definition of the area 44 seed region has a sound biological basis (cf. Eickhoff et al., 2006a), with currently no available alternative based on in vivo imaging (but see Walters et al., 2007 for a potential future perspective). In addition, we also performed a supplementary parcellation with a more conservative definition of left area 44 based on the 50% probability map that was constrained to the surface of the pars opercularis of the inferior frontal gyrus.

The BrainMap database was used to compute whole-brain co-activation maps for each voxel within the VOI (www.brainmap.org; Fox and Lancaster, 2002; Laird et al., 2005, 2009a, 2011). BrainMap is an established database in which the activation foci of many thousand neurominaging experiments are recorded. Each experiment is furthermore coded in terms of behavioral domains and paradigm classes using a standardized taxonomy. Only fMRI and PET experiments from "normal mapping" studies (no interventions, no group comparisons) in healthy subjects that reported results as coordinates in stereotaxic space were included in the analysis. Based on these criteria, approximately 7200 functional neuroimaging experiments were available for the current analysis. The idea of the co-activation analysis is to compute

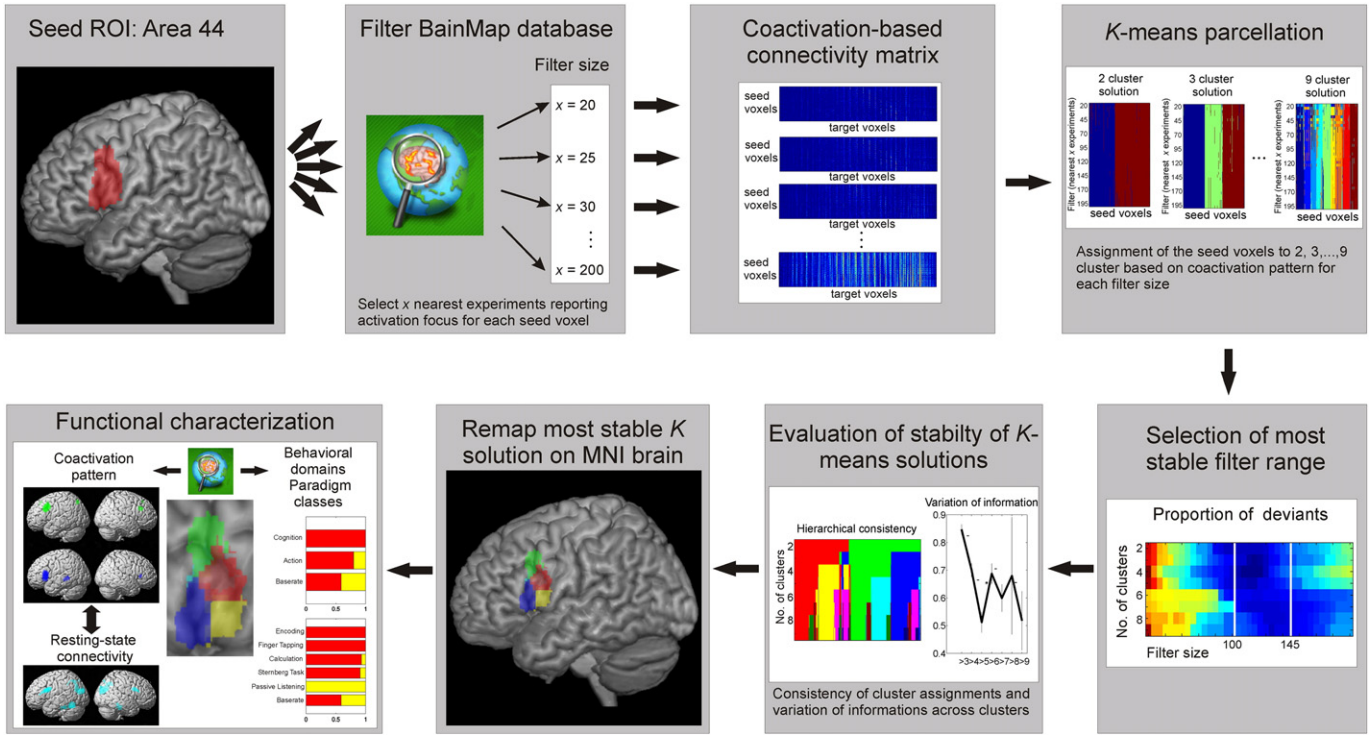

Fig. 1. Summary of analysis steps. For each voxel of area 44, activation foci from the *x* nearest experiments are selected from the BrainMap database. In the next step, the activation foci from the selected experiments are used to generate the brain-wide co-activation profile for each seed voxel and each filter size *x* based on meta-analytic co-activation modeling. Subsequent parcellation of the co-activation matrices was performed with *K*-means. Next, the optimal range of filter sizes was selected based on the consistency of the cluster assignments. The ensuing evaluation of the *K*-means solutions was limited to the optimal filter range. The most stable *K*-means solution was mapped back on the brain and the *K* clusters were functionally characterized based on their connectivity pattern and BrainMap meta-data. See methods for details.

the convergence across (all foci of) all BrainMap experiments where the seed voxel in question is reported as active. However, a general problem of this meta-analytic co-activation mapping approach is that usually not every voxel is activated by a sufficiently high number of experiments (Bzdok et al., 2012a; Cieslik et al., 2012). Therefore, to enable a reliable delineation of task-based functional connectivity, we pooled across the neighborhood of each seed voxel and identified those experiments from the BrainMap database that reported activation closest to the current seed voxel. Importantly, the extent of this spatial filter was systematically varied from including the closest 20 to 200 experiments in steps of five. That is, we selected 20, 25, 30, 35,…, 200 experiments reporting the closest activation at a given seed voxel. This was achieved by calculating and subsequently sorting the Euclidian distances between a given seed voxel and any activation reported in BrainMap. In the following step, the *x* nearest activation foci were selected, as defined by the spatial filter size. Examination of the resulting distances showed that this procedure identified activation foci within close vicinity of the seed voxel. Specifically, the average distance between the seed voxel and activation foci included for that voxel varied from 3.08 mm (i.e. ~1.5 voxels) when 20 experiments were included to 6.53 mm (i.e. ~3 voxels) when 200 experiments were included. Furthermore, although these distances were somewhat larger for seed voxels located in the lateral part than for voxels in more medial parts of area 44, these regional differences were rather moderate (see also Supplementary Figs. S1 and S2).

The retrieved experiments were then used to compute the brain-wide co-activation profile of a given seed voxel for each of the 37 filter sizes. In particular, we performed a coordinate-based meta-analysis over all foci reported in these experiments to quantify their convergence. Since the experiments were identified by activation in or near a particular seed voxel, highest convergence will evidently be found at the location of the seed. Convergence outside the seed, however, indicates co-activation across task-based functional neuroimaging experiments. The brain-wide co-activation pattern for each individual seed voxel thus was computed by activation likelihood estimation (ALE; Eickhoff et al., 2009b; Laird et al., 2009a; Turkeltaub et al., 2002) meta-analysis over the experiments that were associated with that particular voxel by the procedure outlined above. The key idea behind ALE is to treat the foci reported in the associated experiments not as single points, but as centers for 3D Gaussian probability distributions that reflect the spatial uncertainty associated with neuroimaging results. For each experiment, the probability distributions of all reported foci were then combined into a modeled activation (MA) map for that particular experiment (Turkeltaub et al., 2012). The voxel-wise union of these values (across all experiments associated with a particular seed voxel) then yielded an ALE score for each voxel of the brain that describes the co-activation probability with the current seed voxel of each particular location in the brain. The ALE scores of all voxels within the gray matter (based on 10% probability according to the ICBM [International Consortium on Brain Mapping] tissue probability maps) were then recorded before moving to the next voxel of the seed region. It should be noted that this co-activation profile was not thresholded because no inference was sought at this point of the analysis. Rather, the aim was to record for each seed voxel the 'full' individual probability of co-activation with any other voxel and use this profile to parcellate the seed region.

Connectivity-based parcellation

The unthresholded brain-wide co-activation profiles for all seed voxels were then combined into a $N_S \times N_T$ co-activation matrix, where N_S denotes the number of seed voxels in left area 44 (1574 voxels) and N_T the number of target voxels in the reference brain volume at $2 \times 2 \times 2$ mm^3 resolution (~260,000 voxels located within gray matter). Importantly, we computed 37 individual co-activation maps, each representing the connectivity of the different seed voxels when using the 37 different filter sizes (see above). The parcellation of the VOI was performed using *K*-means clustering as implemented in Matlab with $K = 2, 3, \ldots, 9$ using one minus the correlation between the connectivity patterns of the individual seed voxels as the distance measure (correlation distance). Importantly, this parcellation was performed for each of the 37 filter sizes independently, yielding 8 (*K* number of clusters) × 37 (filter size) independent cluster solutions. *K*-means clustering is a non-hierarchical clustering method that uses an iterative algorithm to separate the seed region into a previously selected number of *K* non-overlapping clusters (Hartigan and Wong, 1979). *K*-means aims at minimizing the variance within clusters and maximizing the variance between clusters by first computing the centroid of each cluster and subsequently reassigning voxels to the clusters such that their difference from the centroid is minimal. The reason for using *K*-means rather than hierarchical clustering which preserves the hierarchical consistency by design is that the latter analysis is very sensitive to local features, as clusters cannot change anymore once assigned. This may lead to locally optimal groupings but globally non-optimal solutions. Moreover, hierarchical clustering has one additional degree of freedom, since both distance metric and agglomeration approach need to be specified. We therefore decided to use *K*-means for the parcellation but as we also wanted to ensure that the clusters are hierarchically consistent, we used a pseudo-hierarchical *K*-means clustering by removing hierarchically inconsistent voxels from the clusters obtained by *K*-means. For each of the 8 × 37 parcellations we recorded the best solutions from 25 replications with randomly placed initial centroids.

Selection of optimal filter range

For each of the 37 filter sizes, the *K*-means procedure described above thus yielded eight different solutions parcellating area 44 into two, three, … up to nine subdivisions. One of the challenges of *K*-means clustering is the choice of the optimal cluster solution. This problem is even more complex for the current MACM-based parcellation approach because not only the optimal number of *K* clusters has to be determined. Rather, the use of multiple spatial filter sizes also leads to 37 different solutions that have to be combined into a single parcellation. In previous parcellation studies involving MACM and multiple filters this issue has been dealt with by averaging across all filter sizes (Bzdok et al., 2012a; Cieslik et al., 2012). Here, however, we examined the properties of these various solutions and selected the most stable range of filter sizes. That is, we implement a two-step procedure that involves first a decision on those filter sizes (from the broad range of processed ones) to be included in the final analysis and subsequently a decision on the optimal cluster solution. The first step was based on the consistency of the cluster assignment for the individual voxels across the different filter sizes. We selected the filter range with the lowest number of deviants, i.e., voxels that were assigned differently as compared to the solution from the majority of filters. In other words, we identified those filter sizes which produced solutions most similar to the consensus-solution (sample mode across all filter sizes, i.e., the cluster a voxel was most frequently assigned to) across all filter sizes. The proportion of deviants (normalized within each cluster solution *K*) illustrated in Fig. 2A indicates that most deviants were present in parcellations based on small but also very large filter sizes. We chose the borders of the filter range (100 to 145) based on the increase in (z-normalized) number of deviants before and after these values (Fig. 2B). Of note, the range from the nearest 100 to 145 experiments featured average distances between the seed voxel and assigned activation foci from BrainMap experiments of 2.5 to 3 voxels (see Fig. S1). These distances correspond well to smoothing filters of approximately 5 mm which are standard kernel sizes used in neuroimaging studies and also commonplace for region of interest (ROI) analyses or time-series extractions. We would assume that this optimal range of filter sizes/smoothing reflects the best available compromise between specificity and quantity of the available data. In all subsequent steps the analysis was then restricted to *K* parcellations based on co-activation in the nearest 100 to 145

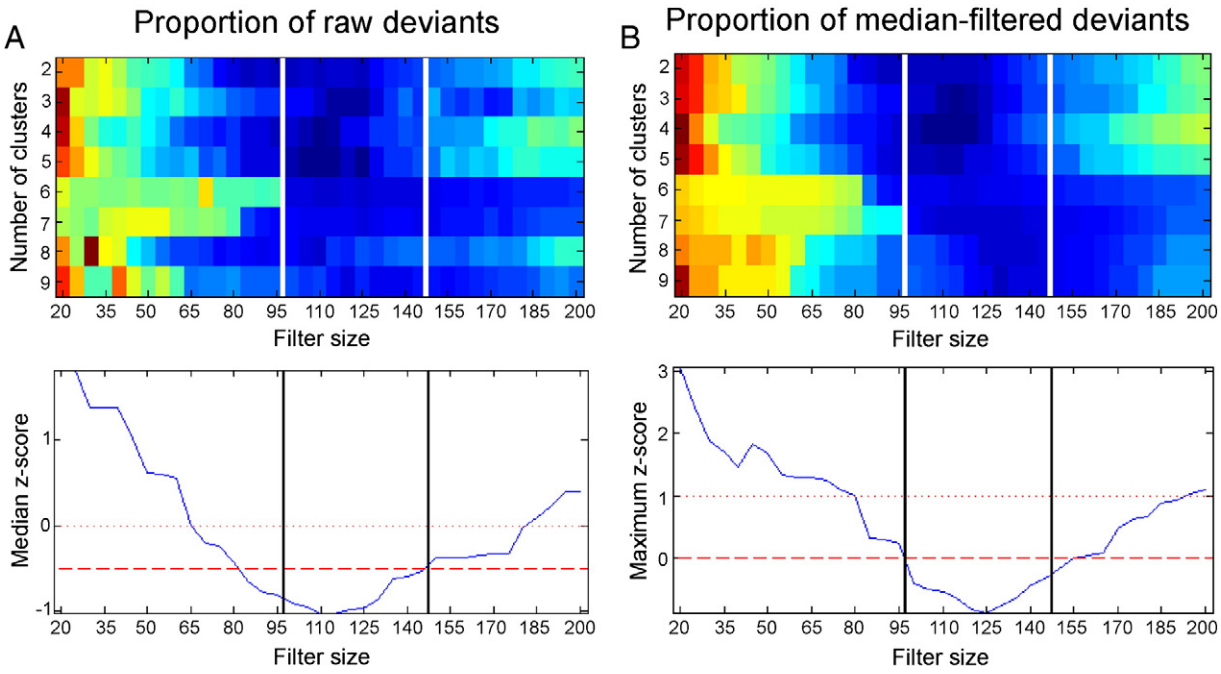

Fig. 2. Deviants and stability. Z-scores on median-filtered deviants (normalized for *K*). The vertical lines specify the ultimately selected, most stable range of filter size (i.e. range with least deviants across *K*). A) The proportion of deviants computed across filter size. Warm colors indicate high numbers of deviants, cold colors indicate low numbers of deviants. B) Maximum z-score of median-filtered deviants.

experiments. However, since the definition of the filter range is not entirely objective, we additionally examined the impact of broadening and narrowing the range on the cluster assignment.

Selection of the optimal number of clusters

Next, we determined the optimal solution of *K* clusters (restricted to the filter sizes between 100 and 145 as outlined in the previous paragraph). We considered three criteria reflecting topological and information-theoretic characteristics of the respective cluster solutions. The first topological criterion was the percentage of voxels not related to the dominant parent cluster compared to the $K-1$ solution (Fig. 3A). This measure is related to the hierarchy-index (Kahnt et al., 2012) and corresponds to the number of lost voxels when only voxels consistent across the entire hierarchy are considered for the final clustering. That is, voxels assigned e.g. to cluster 3 in the $K=3$ solution stemming from a subset of voxels previously assigned to cluster 2 (in the $K=2$ solution) would be excluded if the majority of cluster 3 voxels actually stemmed from cluster 1 (in the $K=2$ solution). A given *K* cluster parcellation qualified as a good solution if the percentage of lost voxels was below the median across all steps and the following clustering step featured a local maximum in the percentage of lost voxels. For example, if (1) moving from a 3- to a 4-cluster solution resulted in a local maximum of lost voxels and (2) the percentage of lost voxels in the 3-cluster solution is lower than the median value (computed across all *K* solutions), the 3-cluster solution would be considered a suitable one. The second topological criterion concerned the number of consistent voxels per cluster, i.e., the sizes of the individual cluster after removal of hierarchically inconsistent voxels (previous criterion). *K* parcellations were evaluated by considering the proportion of the minimum cluster size to the average cluster size provided by a given *K* solution (Fig. 3B). Good solutions were those where the size of the minimum cluster size was more than half of the average cluster size within the *K* solution. In particular, however, solutions in which the smallest cluster becomes zero would have been disregarded, as these indicate that at least one cluster did not contain any hierarchically consistent voxels anymore. Finally, as an information-theoretic criterion, we assessed the similarity of cluster assignments between the current solution and the neighboring ($K-1$ and $K+1$) solutions by using the variation of information (VI) metric (Meila, 2007; Fig. 3C). The VI metric is an established clustering criterion that has previously been used for determining the optimal *K*-means parcellation of a given brain region by Kelly et al. (2010) and Kahnt et al. (2012). For each filter size, the VI metric was computed between a given *K* solution and the subsequent $K+1$ solution. The variation of information between the two cluster solutions *C* and *C′* was computed as

$$VI\left(C,C'\right)_k = H(C)_k + H\left(C'\right)_k - 2I\left(C,C'\right)_k$$

where *H* represents the amount of information (entropy) present in the cluster solutions *C* and *C′*, respectively, and *I* is the mutual information shared by the two cluster solutions *C* and *C′*. Solutions were considered stable if there was a significant increase in VI from the current to the subsequent set of solutions (primary criterion) or if there was a significant decrease from the previous to the current clustering step (secondary criterion).

Visualization of the best cluster solution

The above criteria identified a 5-cluster solution as the most stable parcellation of left area 44 based on co-activation differences within this cytoarchitectonically defined area (see Fig. 3). We only considered hierarchically and spatially consistent voxels located in gray matter for the subsequent analyses. These restrictions resulted in a voxel number of 1251 out of the originally 1574 voxels attributed to left area 44 in the MPM (178 voxels were hierarchically not consistent, 144 were located outside the gray matter and one voxel was lost because it was spatially unconnected to its cluster). We used multidimensional scaling (MDS) to visualize the cluster separation (dissimilarity in whole-brain co-activation profiles). MDS allows the visualization of signals residing in an N-dimensional 'functional space' in 2D. To this end, we first computed for each of the 10 filter sizes the $N_S \times N_S$ distance matrix represented by one minus the pairwise correlation between the co-activation profiles of the

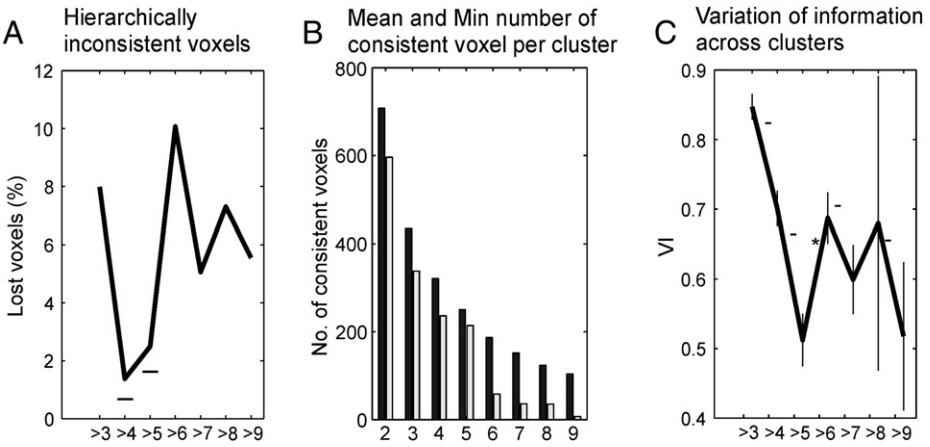

Fig. 3. Cluster criteria. A) Percentage of voxels not related to dominant parent cluster compared to the $K-1$ solution. $K=4$ and $K=5$ are considered good solutions (—) because they are located before the maximum and are lower than the median across all k solutions. B) Mean number of consistent voxel across cluster (dark gray) and the number of voxels of the smallest individual cluster (light gray). The ratio between the minimum and the average cluster size was more than 0.5 for $K=2$, $K=3$, $K=4$ and $K=5$ (good solutions). The ratio was largest for the $K=5$ solution. C) Variation of information between cluster solutions, significant increase in VI (*) to the subsequent cluster solution only for $K=5$ (primary criterion); significant decrease (−) from previous cluster solution for $K=4$, $K=5$, $K=7$, $K=9$ (secondary criterion).

individual seed voxels (correlation distance, as in the *K*-means cluster analysis). Next, we performed MDS on the eigenimage of the distance matrices using Sammon's nonlinear mapping as the goodness-of-fit criterion. In addition, the locations of the five clusters (mode across selected filter size) were mapped back on the brain to visualize their anatomical location.

Post-hoc analysis on task-dependent connectivity: co-activations

To characterize the functional connectivity of the five clusters, a follow-up meta-analytic connectivity modeling (MACM) analysis was performed to determine the co-activation pattern of the individual clusters. The co-activation pattern for each cluster was obtained by first identifying all experiments in the BrainMap database that featured at least one focus of activation in the particular CBP-derived cluster. Next, an ALE meta-analysis was performed on these experiments as described above. In contrast to the MACM underlying the co-activation-based parcellation, where ALE maps were not thresholded to retain the complete pattern of co-activation likelihoods, statistical inference was now performed. To establish which regions were significantly co-activated with a given cluster, ALE scores for the MACM analysis of this cluster were compared to a null-distribution reflecting a random spatial association between experiments with a fixed within-experiment distribution of foci (Eickhoff et al., 2009b). This random-effects inference assesses above-chance convergence between experiments, not clustering of foci within a particular experiment. The observed ALE scores from the actual meta-analysis of experiments activating within a particular cluster were then tested against the ALE scores obtained under this null-distribution yielding a p-value based on the proportion of equal or higher random values (Eickhoff et al., 2012). The resulting non-parametric p-values were transformed into Z-scores and thresholded at a cluster-level FWE-corrected threshold of $p<0.05$ (cluster-forming threshold at voxel-level $p<0.001$).

To identify co-activation common to all clusters, we computed the overlap between the brain-wide co-activation patterns of the five connectivity-derived clusters using a minimum-statistic conjunction (Nichols et al., 2005; conjunction null), i.e., by computing the intersection of the thresholded ALE maps (Caspers et al., 2010). Next, we tested for differences in co-activation patterns between all pairs of clusters by performing MACM separately on the experiments associated with either cluster and computing the voxel-wise difference between the ensuing ALE maps. All experiments contributing to either analysis were then pooled and randomly divided into two groups of the same size as the two original sets of experiments defined by activation in the first or second cluster (Eickhoff et al., 2011). ALE scores for these two randomly assembled groups were calculated and the difference between these ALE scores was recorded for each voxel in the brain. Repeating this process 10,000 times then yielded a null-distribution of differences in ALE scores between the MACM analyses of the two clusters. The 'true' difference in ALE scores was then tested against this null-distribution yielding a posterior probability that the true difference was not due to random noise in an exchangeable set of labels based on the proportion of lower differences in the random exchange. The resulting probability values were then thresholded at $p>0.95$ (95% chance for true difference) and inclusively masked by the respective main effects, i.e., the significant effects in the MACM for the particular cluster. Finally, we computed the specific co-activation pattern for all five clusters, that is, brain regions significantly more co-activated with a given cluster than with any of the other clusters. This was achieved by performing a conjunction analysis (conjunction null) over the differences between a given cluster and the other four ones.

Post-hoc analysis on task-independent connectivity: "resting state"

To cross-validate the pattern of task-dependent co-activation for the delineated clusters within left area 44, we additionally assessed their specific functional connectivity in a task-free setting using resting state correlations. Resting state fMRI images of 153 healthy volunteers (mean age 41.1 ± 18.0 years; 92 males) from the NKI/Rockland sample were obtained through the 1000 functional connectomes project (www.nitrc.org/projects/fcon_1000/; Nooner et al., 2012). During the resting state scans the subjects were instructed to keep their eyes closed and to think about nothing in particular but not to fall asleep (which was confirmed by post-scan debriefing). For each subject 260 resting state EPI images were acquired on a Siemens TimTrio 3 T scanner using blood-oxygen-level-dependent (BOLD) contrast [gradient-echo EPI pulse sequence, TR = 2.5 s, TE = 30 ms, flip angle = 80°, in plane resolution = 3.0 × 3.0 mm^2, 38 axial slices (3.0 mm thickness) covering the entire brain]. The first four scans were excluded from further processing analysis using SPM8 to allow for magnet saturation. The remaining EPI images were first corrected for movement artifacts by affine registration using a two pass procedure in which the images were first aligned to the initial volumes and subsequently to the mean after the first pass. The obtained mean EPI of each subject was then spatially normalized to the MNI single subject template using the 'unified segmentation' approach (Ashburner and Friston, 2005). The ensuing deformation was applied to the individual EPI volumes. To improve

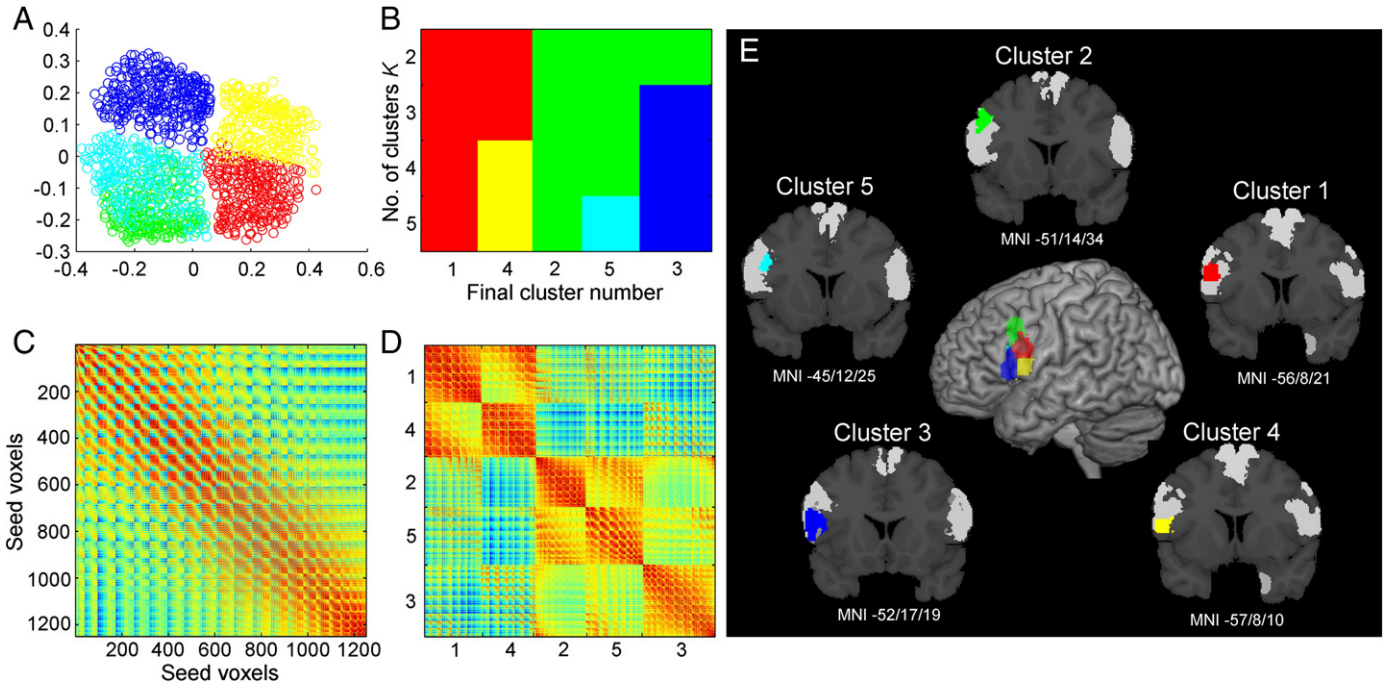

Fig. 4. Visualization and localization of the best cluster solution ($K = 5$). A) Visualization of the 5-cluster solution by multidimensional scaling. Higher proximity between points (voxels) indicates more similar co-activation patterns of these voxels. B) Pattern of cluster assignment and splitting of clusters across levels of *K*. C) Original similarity matrix of the seed voxels. D) Similarity matrix of the seed voxels reordered according to the splitting scheme derived from *K*-means clustering illustrated in B) above. E) The 5-cluster solution is rendered on the brain surface (middle), note that the cyan cluster is located behind the green and the red cluster. The coronal sections display the location of the clusters on the anatomical template of area 44 (left light gray area). Only hierarchically and spatially consistent voxels are included in these visualizations. Color code in A) and B): red = cluster 1, green = cluster 2, blue = cluster 3, yellow = cluster 4, cyan: cluster 5. MNI coordinates correspond to the center of gravity of the clusters.

signal-to-noise ratio and compensate for residual anatomical variations images were smoothed with a 5-mm FWHM Gaussian.

The time-series data of each voxel were processed as follows (Jakobs et al., 2012; Weissenbacher et al., 2009): In order to reduce spurious correlations, variance that could be explained by the following nuisance variables was removed: i) the six motion parameters derived from the image realignment, ii) the first derivative of the realignment parameters, iii) mean gray matter, white matter and CSF signal per time-point as obtained by averaging across voxels attributed to the respective tissue class in the SPM8 segmentation (Reetz et al., 2012; Sommer et al., 2012). All nuisance variables entered the model as first and second order. Data was then band pass filtered preserving frequencies between 0.01 and 0.08 Hz, since meaningful resting state correlations will predominantly be found in these frequencies given that the BOLD response acts as a low-pass filter (Biswal et al., 1995; Fox and Raichle, 2007; Greicius et al., 2003).

We used the five CBP-derived clusters as seeds for the resting state analysis. Linear (Pearson) correlation coefficients between the time series of the seed regions and all other gray matter voxels in the brain were computed to quantify resting state functional connectivity (Reetz et al., 2012; zu Eulenburg et al., 2012). These voxel-wise correlation coefficients were then transformed into Fisher's Z-scores and tested for consistency in a flexible factorial model across subjects. The main effect of connectivity for each cluster as well as contrasts between the clusters was tested using the standard SPM8 implementations with the appropriate non-sphericity correction. In correspondence with the task-dependent MACM co-activation analysis above, we firstly computed a conjunction across the main effect of positive connectivity of the five clusters, i.e., the task-free functional connectivity shared by all five clusters. Secondly, we performed a conjunction analysis for each cluster across the contrasts with the four other clusters corresponding to the specific co-activation pattern of each cluster. These conjunction analyses were based on the minimum t-statistic (conjunction null; Nichols et al., 2005) and thresholded at $p < 0.05$ (FWE-corrected at cluster level; cluster-forming threshold at voxel-level $p < 0.001$). For comparison and visualization purposes, the resting state conjunctions were masked with the corresponding MACM connectivity results.

Post-hoc functional characterization: meta-data

The functional characterization of the CBP-derived clusters was based on the 'Behavioral Domain' and 'Paradigm Class' meta-data categories available for each neuroimaging experiment included in the BrainMap database. Behavioral domains include the main categories cognition, action, perception, emotion, and interoception, as well as their related sub-categories. Paradigm classes categorize the specific task employed (see http://brainmap.org/scribe for more information on the BrainMap taxonomy and Supplementary Table S1 and S2 for complete lists of BrainMap Behavioral Domains and Paradigm Classes).

In the first step, we determined the individual functional profile of the five CBP-derived clusters by using forward and reverse inference. Forward inference is the probability of observing activity in a brain region given knowledge of the psychological process, whereas reverse inference is the probability of a psychological process being present given knowledge of activation in a particular brain region. In the forward

Table 1
Co-activated regions: conjunction across the five clusters.

Region	Overlap with cytoarchitectonic area	x	y	z	Cluster size
L IFG/precentral gyrus/insula	Area 44[a] (36% overlap)	−52	10	20	938
R IFG/precentral gyrus		48	10	30	16
R insula		36	20	0	214
L/R SMA/MCC	Area 6[b] (47% overlap)	−2	8	52	647
L thalamus		−12	−14	6	43
R thalamus		10	−12	6	4
L putamen		−20	2	6	15

x, y, z coordinates refer to the peak voxel in MNI space. R, right; L, left.
[a] Amunts et al., 1999.
[b] Geyer, 2004.

inference approach, a cluster's functional profile was determined by identifying taxonomic labels, for which the probability of finding activation in the respective cluster was significantly higher than the overall chance (across the entire database) of finding activation in that particular cluster. Significance was established using a binomial test ($p < .05$, corrected for multiple comparisons using Bonferroni's method; Eickhoff et al., 2011; Laird et al., 2009b; Nickl-Jockschat et al., 2012). That is, we tested whether the conditional probability of activation given a particular label [P(Activation|Task)] was higher than the baseline probability of activating the region in question per se [P(Activation)]. In the reverse inference approach, a cluster's functional profile was determined by identifying the most likely behavioral domains and paradigm classes given activation in a particular cluster. This likelihood P(Task|Activation) can be derived from P(Activation|Task) as well as P(Task) and P(Activation) using Bayes rule. Significance (at $p < 0.05$, corrected for multiple comparisons using Bonferroni's method) was then assessed by means of a chi-squared test.

Secondly, we contrasted the functional profiles of the clusters at each level of splitting up to the most stable 5-cluster solution. More precisely, we always contrasted the newly emerged child cluster with its remaining parent cluster at the same level of K. Thus, we compared cluster $1_{K=2}$ with cluster $2_{K=2}$, cluster $3_{K=3}$ with cluster $2_{K=3}$, cluster $4_{K=4}$ with cluster $1_{K=4}$, and cluster $5_{K=5}$ with cluster $2_{K=5}$ (cf. Fig. 4B). For each comparison of the splitting cluster, the analysis was constrained to all BrainMap experiments activating either cluster. From this pool of experiments, the baserate is the a priori probability of any focus to lie in either of the two compared clusters. Forward inference here compared the activation probabilities of the clusters given a task compared to the a priori baserate by means of a binomial test ($p < .05$, corrected for multiple comparisons using Bonferroni's method). In the likewise performed reverse inference approach, we compared the occurrence probabilities of the tasks given activation in the one cluster (rather than in the other cluster) and assessed them by means of a chi-squared test ($p < .05$, corrected for multiple comparisons using Bonferroni's method).

Results

Best cluster solution and stability of the clustering

Based on the consistency of the cluster assignment for the individual voxels across the different filter sizes, we only considered the closest 100 to 145 experiments (Fig. 2). The topographical and information-theoretic criteria (Fig. 3) then identified the 5-cluster solution as the best one among the 8 assessed levels of K-means clustering (from $K = 2$ to $K = 9$). The visualization in 2D, the hierarchical splitting of the five clusters and their anatomical location in the brain are displayed in Fig. 4. The clusters were labeled from 1 to 5 based on the hierarchical splitting order. At $K = 2$, left area 44 was composed of a posterior cluster $1_{K=2}$ and an anterior cluster $2_{K=2}$. At the next level $K = 3$, the posterior cluster $1_{K=2}$ remained the same but from the anterior cluster $2_{K=2}$ the ventral portion comprising the final cluster 3 split off. At $K = 4$, the final cluster 4 emerged from the posterior cluster $1_{K=2}$ ventrally. The remaining dorsal portion contained the final cluster 1. At the last split at $K = 5$, the final cluster 5 emerged from the anterior parent cluster $2_{K=3}$. Cluster 5 was located in close vicinity of the inferior frontal junction and the final cluster 2 was located dorsally extending into the inferior frontal sulcus.

To ascertain that the selected definition of the filter range including only the closest 100 to 145 experiments did not overtly impact the results, we additionally examined the effect of both broadening and narrowing the filter range by three steps on both sides, i.e., including 15 additional/fewer experiments per voxel. The results showed that cluster assignments of the individual voxels were identical to the cluster assignment of the selected filter range (100 to 145) for 96.3% of the voxels in the broadened range (85 to 160) and for 94.2% of the voxels in the narrowed range (115 to 130) across all eight parcellation levels ($K = 2$ to $K = 9$). Importantly, the 5-cluster solution was identified as the most optimal solution for both the broadened and the narrowed range. Comparison of the cluster assignments across these selected $K = 2$ to $K = 5$ parcellation levels showed that these were identical to those of the 5-cluster solution based on the selected filter range for 99.0% (broadened range) and 98.4% (narrowed range) of the voxels, respectively. Very similar results with identical cluster assignments between 88% and 99% were obtained when broadening or narrowing the filter range asymmetrically and when broadening and narrowing the filter range by two steps or one step. Together, these results clearly demonstrate that the cluster assignment is extremely stable across choice of filter-ranges for further analysis and accordingly the exact definition of the filter range should not affect the final parcellation results.

Furthermore, we performed a supplementary parcellation based on the 50% probability map of left area 44 to ensure that the parcellation results are not driven by surrounding regions into which the rather liberal MPM definition may be partly extending. This more conservative VOI was limited to those regions on the opercular surface of the left inferior frontal gyrus in which the probability for area 44 was at least 50%. It was hence considerably smaller and focused on the center of left area 44, accordingly, it did not include the inferior frontal junction anymore (Supplementary Fig. S3). The parcellation results demonstrated that a 4-cluster solution was the

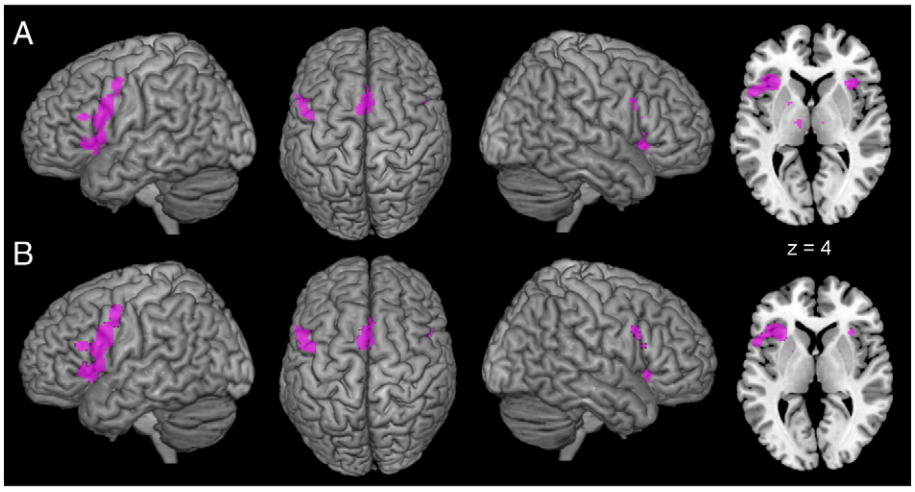

Fig. 5. Conjunction of connectivity across clusters 1–5. A) Regions significantly co-activated with all five clusters. B) Regions showing significant resting-state connectivity with all five clusters (masked with common MACM connectivity from A).

optimal parcellation for this VOI, the fifth cluster present in the main analysis had disappeared because of the exclusion of the inferior frontal junction part. However, the anatomical location of these four clusters corresponded extremely well to those of clusters 1 to 4 from the main analysis based on the MPM (Fig. S4 and S5). Additionally, we still identified a posterior-anterior splitting at the $K = 2$ level as we did for the 5-cluster solution based on the MPM. Moreover, both the anterior and the posterior cluster were split into a dorsal and ventral part, reflecting the same splitting pattern as in the main analysis. In the light of very similar moderate distances between seed voxels and activation foci as in the main parcellation (obtained average distances in the supplementary parcellation varied from 3.08 mm (i.e. ~1.5 voxels) when 20 experiments were included to 6.62 mm (i.e. ~3 voxels) when 200 experiments were included) and the fact that the 50% probability map of area 44 is much smaller than the MPM used in the main analysis (733 vs. 1574 voxel), it seems very unlikely that neighboring regions of area 44 are driving the supplementary parcellation. The high similarity between both parcellations thus supports the validity of the parcellation based on the more liberal MPM of left area 44 and confirms that cluster assignments and splitting order are present even when restricting the analysis only to the core of histologically defined left area 44.

Post-hoc analysis of co-activation patterns of the clusters

The follow-up MACM analysis on the final clusters was performed to reveal the co-activation pattern for each cluster. A conjunction across the five co-activation patterns identified co-activated regions common to all five clusters. These common co-activations included bilateral inferior frontal gyrus (IFG)/precentral gyrus, insula, supplementary motor area (SMA)/middle cingulate cortex (MCC), thalamus and the left putamen (see Table 1 and Fig. 5A for details including associated cytoarchitectonic areas). This common connectivity was supported by the task-free resting state connectivity analysis (Fig. 5B). In particular, we found all of these connections likewise present in the analysis of task-free functional connectivity except for the thalamus, which barely missed the statistical threshold.

We furthermore examined the specific connectivity pattern of each cluster, that is, brain regions significantly more coupled with a given cluster than with any of the other ones (see Table 2 and Fig. 6A for details including associated cytoarchitectonic areas). Overall, the specific MACM connectivity indicated high local connectivity surrounding any given cluster. Of note, each cluster's right-sided homotope was also specifically co-activated. Additionally, cluster 1 showed a particular co-activation with the bilateral inferior and superior parietal cortex including the supramarginal gyrus (SMG) and the postcentral gyrus, with the superior frontal gyrus (SFG), the precentral gyrus and the supplementary motor area (SMA). Cluster 2 was specifically co-activated with the left posterior intraparietal sulcus (IPS) and with the medial superior frontal gyrus (medSFG). Cluster 3 showed specific task-dependent connectivity with the left posterior middle temporal gyrus (MTG) and with the left hippocampus and amgygdala. For cluster 4, the specific connectivity included the left anterior superior temporal gyrus (STG), the bilateral insula, putamen and thalamus as well as the right SMA. Specific co-activations with cluster 5 were found bilaterally in the anterior inferior parietal lobule (IPL) and with the right insula and pre-SMA/ MCC. The task-free resting state analysis confirmed this specific connectivity pattern of the clusters (see the conjunction of specific resting state and MACM connectivity displayed in Fig. 6B and the non-masked resting state connectivity in Fig. S6), even though the connectivity of cluster 3 with the left hippocampus/amygdala, the connectivity of cluster 4 with the thalamus and the connectivity of cluster 5 with the right insula and with the pre-SMA/ MCC did not quite reach the statistical threshold. Thus, both task-dependent MACM and task-independent resting state connectivity showed converging evidence for functional specific connectivity patterns associated with each of the five clusters.

Post-hoc functional characterization: BrainMap meta-data

We first determined the quantitative forward and reverse inference on the behavioral domains and paradigm classes as recorded in BrainMap for each of the five clusters individually. The significant

Table 2
Co-activated regions: specific connectivity.

Region	Overlap with cytoarchitectonic area	x	y	z	Cluster size
Cluster 1					
L IFG/precentral gyrus	Area 44[a] (41% overlap) Area 6[b] (23% overlap	−60	8	34	582
L postcentral gyrus/SPL/SMG	Area PFt[c] (17% overlap) Area 7A[d] (15% overlap)	−66	−20	24	1049
L SFG/SMA	Area 6[b] (79% overlap)	−16	2	58	119
R IPL/SPL/postcentral gyrus	Area hIP2[e] (18% overlap) Area 7PC[d] (17% overlap)	42	−40	44	393
R SPL	Area 7P[d] (72% overlap) Area 7A[d] (23% overlap)	16	−68	56	173
R IFG/precentral gyrus	Area 44[a] (45% overlap)	58	8	26	346
R SMG/Rolandic operculum	Area OP1[f] (30% overlap) Area PFt[c] (30% overlap) Area PF[c] (16% overlap) Area PFop[c] (16% overlap)	56	−28	38	292
R SFG/precentral gyrus	Area 6[b] (28% overlap) Area 4A[g] (5% overlap)	32	−10	58	155
Cluster 2					
L IFG/MFG	Area 44[a] (35% overlap) Area 45[a] (11% overlap)	−50	12	46	536
L IPS	Area PGa[c] (50% overlap) Area 7A[d] (33% overlap)	−32	−74	54	60
L/R medSFG		0	−34	50	54
R IFG	Area 45[a] (49% overlap)	54	26	30	90
Cluster 3					
L IFG	Area 44[a] (31% overlap) Area 45[a] (30% overlap	−58	25	8	802
L MTG		−60	−40	2	172
L hippocampus/ amygdala	Area CA[h] (49% overlap) Area LB[h] (21% overlap) Area SF[h] (13% overlap)	−24	−10	−16	77
R IFG	Area 45[a] (89% overlap)	48	26	6	78
Cluster 4					
L IFG/STG/insula/ putamen	Area 44[a] (14% overlap) Area OP4[f] (8% overlap)	−56	12	14	1325
L thalamus		−8	−12	16	110
R thalamus		10	−24	4	157
R IFG/insula/putamen	Area 44[a] (19% overlap)	46	12	8	1311
R SMA (area 6)	Area 6[b] (83% overlap)	6	6	66	166
Cluster 5					
L IFG/ precentral gyrus	Area 44[a] (15% overlap) Area 45[a] (6% overlap)	−38	8	38	940
R IFG		36	10	30	70
L IPL	Area hIP3[d] (41% overlap) Area hIP1[e] (10% overlap)	−26	−56	40	340
R IPL	Area hIP3[d] (35% overlap) Area hIP1[e] (31% overlap) Area PGa[c] (13% overlap)	40	−56	44	82
R insula		34	30	0	125
R pre-SMA/MCC	Area 6[b] (7% overlap)	6	18	46	82

All activations $p < .001$; extent threshold of 50 voxels. x, y, z coordinates refer to the peak voxel in MNI space. R, right; L, left.

[a] Amunts et al., 1999.
[b] Geyer, 2004.
[c] Caspers et al., 2006.
[d] Scheperjans et al., 2008.
[e] Choi et al., 2006.
[f] Eickhoff et al., 2006b.
[g] Geyer et al., 1996.
[h] Amunts et al., 2005.

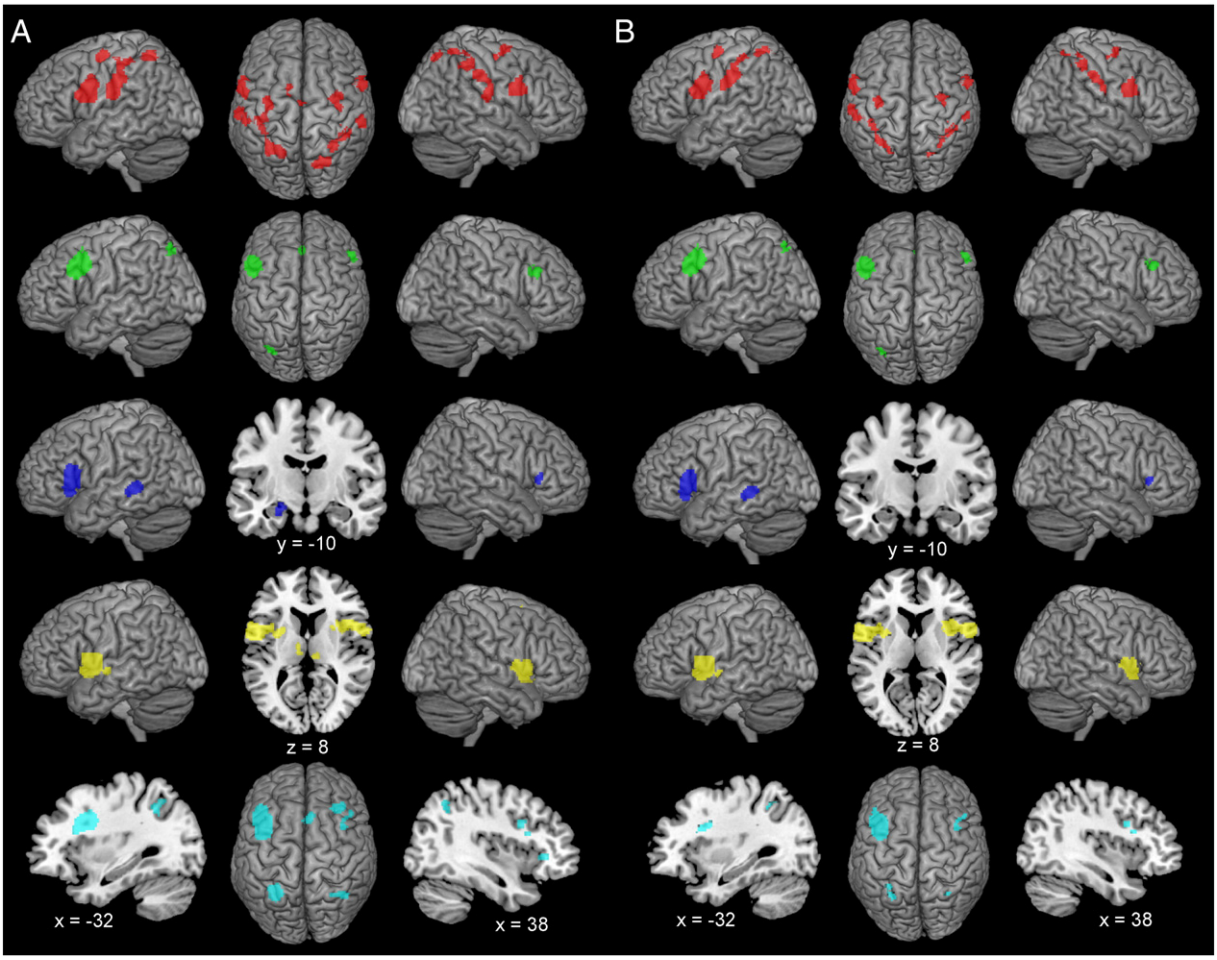

Fig. 6. Specific connectivity pattern of the five clusters. A) Regions significantly more co-activated with a given cluster than with any of the other four clusters. B) Regions showing significantly more resting state connectivity with a given cluster than with any of the other four clusters (masked with specific MACM connectivity from A; for non-masked resting state connectivity see also Fig. S6). Color code: red = cluster 1, green = cluster 2, blue = cluster 3, yellow = cluster 4, cyan = cluster 5.

activation probabilities within a cluster given a certain taxonomic label (forward inference) and the significant probability of domain and paradigm occurrence given activation in a certain cluster (reverse inference) are shown in Fig. 7. Note that the taxonomic terms displayed in Fig. 7 are taken from the BrainMap database and that this individual functional characterization was not based on contrasts between clusters but shows which behavioral domains and paradigm classes are significantly associated with a particular cluster. Furthermore, it should be noted that this inference is constrained by the terms available in the BrainMap database. The behavioral domains and paradigm classes of the individual clusters emphasized the strong association between activation in left area 44 and language-related processes such as phonology, semantics, overt and covert speech. However, these functional profiles also hint at specific characteristics and hence functional differences between the five clusters identified within this histologically defined area. In summary, cluster 1 was significantly associated with phonology, syntax and tasks requiring overt speech but also with action imagination. Cluster 2 was involved in semantics, orthography and covert speech but also in working-memory processes. Cluster 3 was associated with several core aspects of language including overt and covert speech, semantics, phonology and syntax. The profile of cluster 4 indicated primarily a role in action imagination but also in music comprehension and production, making it the only cluster without a significant association to any language-related process. Cluster 5 was involved in speech, phonology and semantics but also in working-memory processes and paradigms requiring task switching and cognitive control (e.g. the stroop task). This functional characterization of the final clusters was confirmed by the supplemental parcellation based on the 50% probability map of left area 44. The functional profiles of the resulting clusters 1 to 4 were very similar to those from the main parcellation (Fig. S7).

To additionally examine the differences between the splitting clusters (that is, differences between the newly emerged child cluster and its remaining parent cluster) we compared the functional profiles of the clusters at each level of splitting (Fig. 8). In this context, please note that the posterior cluster $1_{K=2}$ and the anterior clusters $2_{K=2}$ and $2_{K=3}$ do not correspond to the final CBP-derived clusters 1 and 2. Rather, the posterior cluster $1_{K=2}$ still contains its child cluster 4, the anterior cluster $2_{K=2}$ still contains its child cluster 3 as well as 5 and the anterior cluster $2_{K=3}$ still contains its child cluster 5. The comparison at $K = 2$ revealed that the posterior cluster $1_{K=2}$ was more associated with action imagination and execution as well as with action and body-related perception than the anterior cluster $2_{K=2}$. In contrast, the anterior cluster $2_{K=2}$ showed a higher activation probability for semantics and working memory. At $K = 3$, splitting this anterior cluster $2_{K=2}$, the ventral cluster $3_{K=3}$ differed significantly from the more dorsal cluster $2_{K=3}$ in its association with social cognition. This cluster $2_{K=3}$ on the other hand, showed a higher probability for working memory and several body-related perceptual and cognitive processes than the ventral cluster $3_{K=3}$. Contrasting the posterior-dorsal cluster $1_{K=4}$ with the posterior-ventral cluster $4_{K=4}$ revealed a stronger link of the former with language, tasks requiring overt speech and working memory. The ventral cluster $4_{K=4}$ in turn showed significantly stronger association than cluster $1_{K=4}$ only with regard to a higher

activation probability in passive listening tasks. Finally, the last split at $K = 5$ distinguished a medially located cluster $5_{K=5}$ from cluster $2_{K=5}$ based on a higher activation probability in overt word stem completion tasks of cluster $5_{K=5}$.

Post-hoc external validation

In order to validate the functional characterization of the five clusters, we compared activations within left area 44 as observed in previously conducted fMRI studies from our laboratory with the localization of the delineated clusters. This additional comparison was merely performed to check whether the extent of a given cluster with a presumed functional role is in agreement with the localization and extent of activations from specific experiments. Also note that these five experiments are not included in the BrainMap database and therefore can be regarded as external evidence. For the posterior portion, the results point to a role of the posterior clusters 1 and 4 in the motor network (Kellermann et al., 2012; Fig. 9A), but furthermore they also indicate the specific involvement of the dorsal cluster 1 in phonological word generation (Heim et al., 2008; Fig. 9B) and of the ventral cluster 4 in action imitation (Caspers et al., 2010; Fig. 9C). In addition, search for meaning in degraded speech (Clos et al., 2012; Fig. 9D) and social judgments on faces (Bzdok et al., 2012b; Fig. 9E) both were clearly localized to the anterior-ventral cluster 3. Importantly, these activations were specifically localized to the associated cluster(s) within left area 44, although they partly extended into surrounding regions as well.

Discussion

We demonstrated that cytoarchitectonic left area 44 of Broca's region can be parcellated into five distinct clusters based on different whole-brain co-activation patterns across the wide range of neuroimaging experiments recorded in the BrainMap database. This approach has the advantage over parcellations based on DTI or resting state data in that a functional characterization of the resultant clusters can be obtained based on BrainMap meta-data. We identified the best parcellation in a two-step procedure. Firstly, the optimal range of filter sizes (number of foci included for each voxel) was chosen based on the stability of cluster assignments. It is important to note that slight variations of the exact filter range did not make any notable difference in the subsequent clustering. Secondly, the eight different parcellations derived from *K*-means clustering with *K* varying from 2 to 9 enabled us to identify the 5-cluster parcellation as the best solution based on topographical and information-theoretical criteria as employed in previous CBP applications. Note that this 5-cluster parcellation will be publicly available on the following website http://www.fz-juelich.de/inm/inm-1/EN/Forschung/Brain_Network_Modeling/Brain_Network_Modeling_node.html upon publication of the manuscript. Two kinds of post-hoc analyses on this co-activation-based 5-cluster parcellation were then performed. Firstly, the follow-up MACM analysis on the ensuing five clusters revealed co-activation differences underlying the subparcellation of left area 44. The subsequent cross-validation by task-independent resting state connectivity indicates convergent functional connectivity differences also in a task-free setting. Secondly, the functions of the delineated clusters were quantitatively characterized using the BrainMap meta-data. These post-hoc analyses showed that although all five subregions were linked with language and showed common connectivity to several regions, they also featured clear differences in connectivity and function.

The strongest differentiation within left area 44 was found at the first level of clustering ($K = 2$) where the posterior part more associated with action, and the anterior part, primarily associated with language, separated from each other. This differentiation is in accordance with the receptor-based mapping of Broca's region (Amunts et al., 2010), which revealed a subdivision of area 44 into an anterior-dorsal (44d) and a posterior-ventral (44v) area based on pronounced differences in the concentration of muscarinic M_2, glutamatergic AMPA, and adrenergic $\alpha 1$ receptors. Topographically, our action cluster corresponds to the posterior-ventral area 44v and our language cluster to the anterior-dorsal area 44d.

In addition to this fundamental differentiation within left area 44, the specific co-activations and functional characterization of the final clusters pointed to several differences within the anterior language and the posterior action part, respectively. We subsequently try to summarize and interpret these quantitative results in the light of previous findings in order to highlight the potential functional role of each cluster. It should be noted though that this interpretation is certainly subjective in nature and represents merely a reasoning on the most likely function given the current qualitative findings and previous findings reported in the literature. In the posterior portion the qualitative forward and reverse inference showed that the ventral cluster 4 was most strongly associated with action-related processing whereas the more dorsal cluster 1 showed a relatively stronger association with cognitive functions, in particular language and working-memory processes. Cluster 1 was furthermore associated with tasks requiring overt speech and showed high evidence for phonological processes. This link with phonological processes in overt speech is supported by studies reporting higher activation of the posterior-dorsal area 44 in tasks requiring phonological word generation as compared to either semantic or syntactic word generation (Costafreda et al., 2006; Heim et al., 2008). The connectivity pattern of cluster 1 suggests that this task is accomplished primarily in concert with its right homotope, the inferior and superior parietal cortex, the superior frontal gyrus (SFG), the precentral gyrus and the supplementary motor area (SMA). Indeed, these regions are known to be involved in production of both speech (Brown et al., 2009; Eickhoff et al., 2009a) but also non-speech sounds involving orofacial and vocal tracts movements (Chang et al., 2009). Thus, the posterior-dorsal cluster 1 might contribute specifically to phonological processes and overt articulation of speech.

In contrast, cluster 4 showed a stronger association with action and action imagination than any other cluster, including the dorsally adjacent cluster 1. This finding is in agreement with a meta-analysis indicating that in particular the posterior-ventral part of left area 44 is consistently recruited by action imitation and may hence represent part of the mirror-neuron system (Caspers et al., 2010) as a potential homologue to macaque area F5 (Rizzolatti and Arbib, 1998). Furthermore, the quantitative reverse inference on cluster 4 provided also a link with music perception and production. Presumably, this cluster might be particularly responsive to sequencing aspects, including rhythm-processing, common to both movements and music. Indeed, activation in the posterior-ventral part of area 44 together with the bilateral insula, thalamus and basal ganglia has been reported in response to musical sequences (Koelsch et al., 2002). Moreover, time-keeping and sequencing of motor and auditory listening tasks are also strongly associated with activations in the SMA, insula, putamen and thalamus (Stevens et al., 2007). These findings match the specific co-activation network of cluster 4 and suggest that the posterior-ventral cluster 4 might play a specific role in the rhythmic sequencing.

Within the anterior 'language' part of left area 44, cluster 2 was located more dorsally and showed a significant association with tasks probing working memory, semantics and orthography as well as those involving reading and covert speech. Compared to the more ventrally located cluster 3, cluster 2 was in particular significantly more strongly associated with working memory, but also with cognitive and perceptual non-verbal processes. Furthermore, the specific co-activation of cluster 2 with medial superior and middle frontal gyri and the intraparietal sulcus form a network reliably associated with working memory across verbal and non-verbal domains (Rottschy et al., 2012). These findings are in accordance with a study demonstrating a shift of activation within area 44 superiorly towards the IFS with increasing demands of working memory in language processing (Makuuchi et al., 2009). Together,

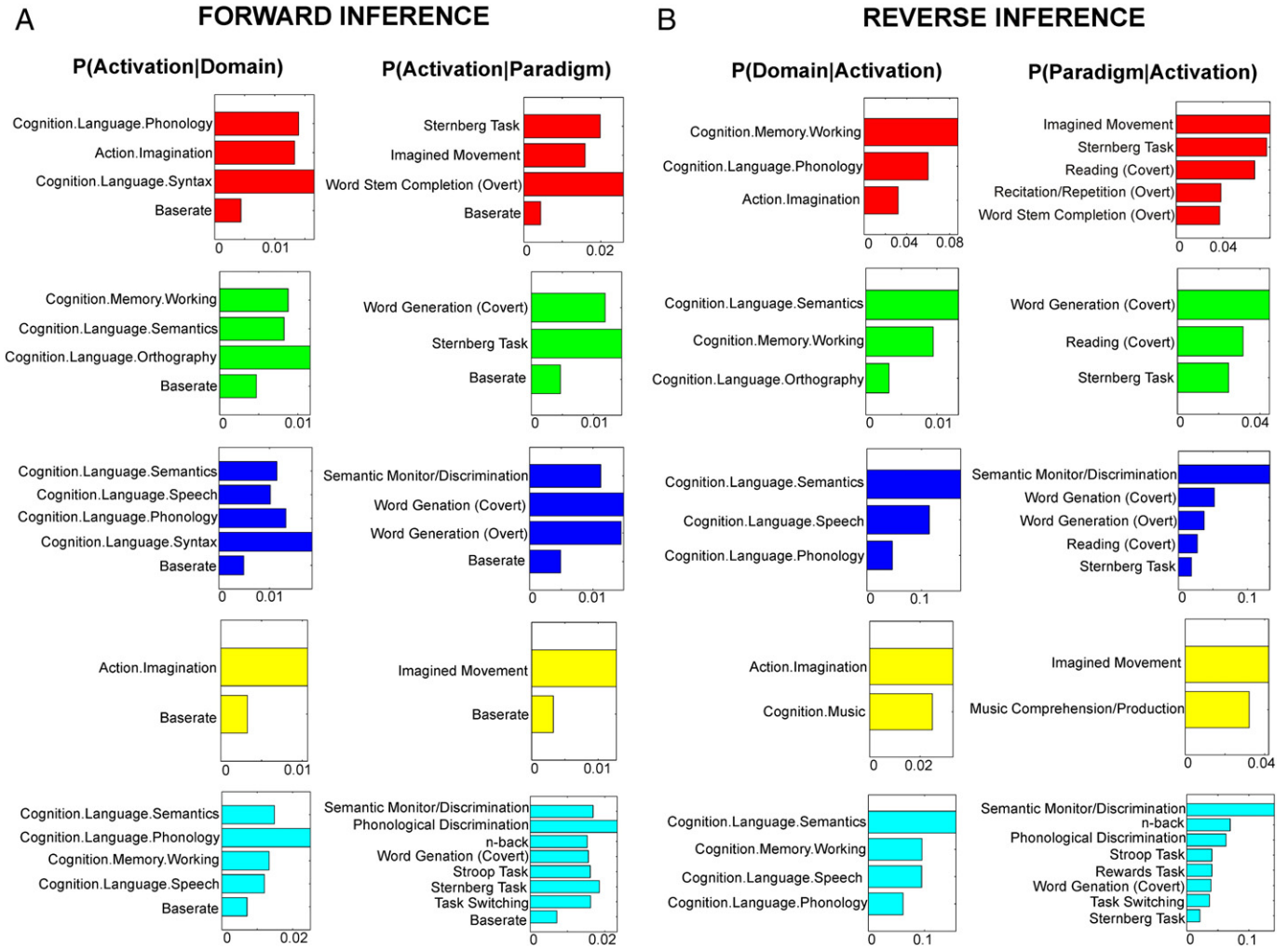

Fig. 7. Behavioral domains and paradigm classes of final clusters. A) Forward inference on final clusters: significant activation probability of the cluster given a certain domain (left column) or paradigm (right column). B) Reverse inference on final clusters: significant probability of domain (left column) or paradigm (right column) occurrence given activation in a cluster. Color code: red = cluster 1, green = cluster 2, blue = cluster 3, yellow = cluster 4, cyan = cluster 5.

these findings support a role of cluster 2 in working-memory mechanisms required for language-related processes including speech perception and orthography but potentially also for other, non-verbal, domains. Whether this cluster belongs to cytoarchitectonically defined area 44 or to dorsally adjacent regions, which are until now unmapped, remains a future project. The localization of this cluster in the posterior inferior frontal sulcus and its involvement in non-verbal processes may be arguments towards an interpretation as an area outside area 44. A putative candidate might be recently reported areas the inferior frontal sulcus (Bradler et al., 2012). Thus, the region of interest as based of the MPM of area 44 in the present study would include non-area 44 compartments. This seems to be also true for cluster 5 (see below).

Ventral-anterior cluster 3 had a very strong association with various key aspects of language processing such as semantics, syntax, phonology and overt as well as covert speech that seemed to be more specific for these verbal-semantic processes than in any other cluster. Contrasting this cluster with cluster 2 demonstrated that cluster 3 was also significantly more involved in social cognition including theory of mind tasks than cluster 2. A possible explanation for the association with both language processes and social cognition might be that most social concepts are rather abstract (Zahn et al., 2007) and therefore most likely represented verbally (Dove, 2010; Wang et al., 2010). Accordingly, tasks involving social cognition might require covert speech mechanisms (Femyhough and Meins, 2009). However, a more likely explanation of this association may be the necessity of access to semantics in the form of previously acquired (verbal and non-verbal) conceptual knowledge that both domains have in common (Binder and Desai, 2011). In particular, social interactions might heavily depend on the recognition of meaningful cues in other people's behavior, gestures and mimic. These non-verbal processes should be phylogenetically much older than verbal mechanisms and therefore might have formed a basis for the ability to decode meaning from speech sounds (Arbib, 2005; Corballis, 2009). Interestingly, in particular the anterior-ventral part of area 44 has been suggested to support speech comprehension by searching for meaning in auditory speech signals (Clos et al., 2012). We would speculate that activations of the anterior-ventral part of area 44 observed in social evaluations of faces (Bzdok et al., 2012b) and in judgments of emotional states of others (Ochsner et al., 2004) reflect a similar search for meaning in the social domain. This interpretation is in accordance with the specific co-activated network of cluster 3 that included besides parts of the cluster's right homotope also the

Fig. 8. Differences in behavioral domains and paradigm classes between splitting clusters.Significant differences in forward (upper panels) and reverse (lower panels) inference between A) cluster 1 and cluster 2 at $K = 2$; B) cluster 2 and 3 at $K = 3$; C) cluster 1 and 4 at $K = 4$; D) cluster 2 and 5 at $K = 5$. Color code: red = cluster 1, green = cluster 2, blue = cluster 3, yellow = cluster 4, cyan = cluster 5.

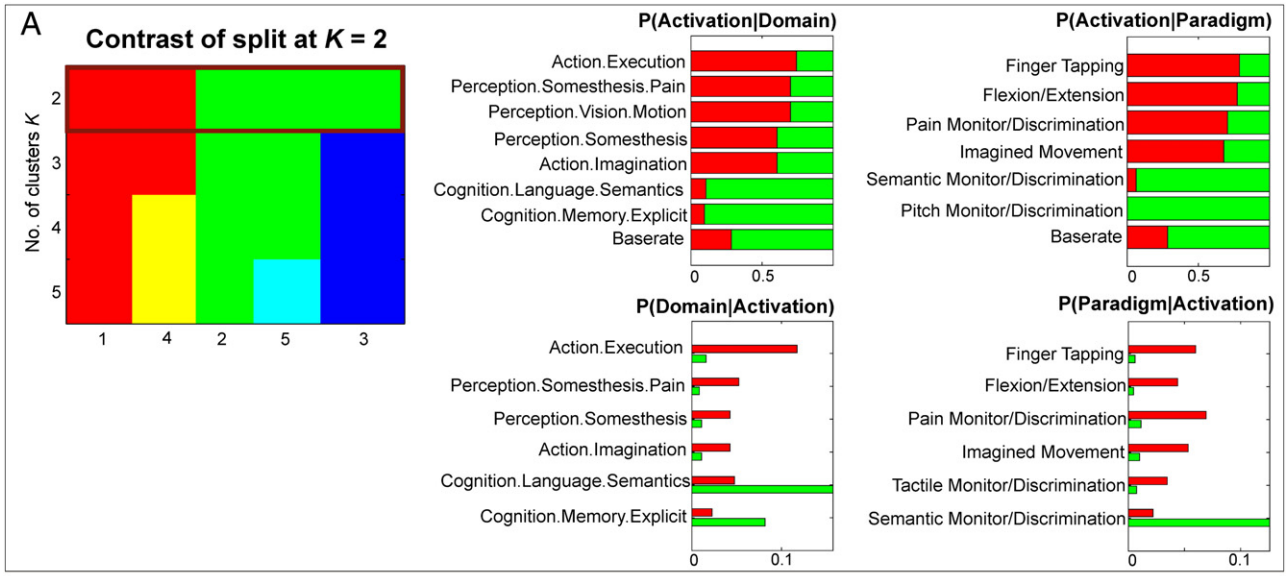
A
Contrast of split at K = 2
No. of clusters K
2
3
4
5
1 4 2 5 3
P(Activation|Domain)
Action.Execution
Perception.Somesthesis.Pain
Perception.Vision.Motion
Perception.Somesthesis
Action.Imagination
Cognition.Language.Semantics
Cognition.Memory.Explicit
Baserate
0 0.5
P(Activation|Paradigm)
Finger Tapping
Flexion/Extension
Pain Monitor/Discrimination
Imagined Movement
Semantic Monitor/Discrimination
Pitch Monitor/Discrimination
Baserate
0 0.5
P(Domain|Activation)
Action.Execution
Perception.Somesthesis.Pain
Perception.Somesthesis
Action.Imagination
Cognition.Language.Semantics
Cognition.Memory.Explicit
0 0.1
P(Paradigm|Activation)
Finger Tapping
Flexion/Extension
Pain Monitor/Discrimination
Imagined Movement
Tactile Monitor/Discrimination
Semantic Monitor/Discrimination
0 0.1

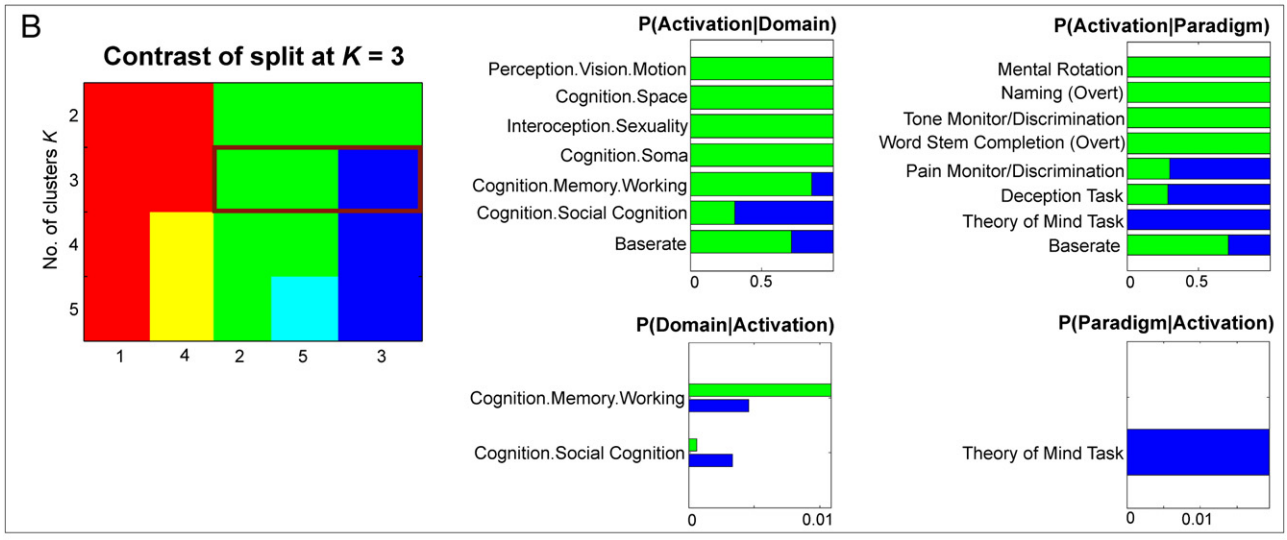
B
Contrast of split at K = 3
No. of clusters K
2
3
4
5
1 4 2 5 3
P(Activation|Domain)
Perception.Vision.Motion
Cognition.Space
Interoception.Sexuality
Cognition.Soma
Cognition.Memory.Working
Cognition.Social Cognition
Baserate
0 0.5
P(Activation|Paradigm)
Mental Rotation
Naming (Overt)
Tone Monitor/Discrimination
Word Stem Completion (Overt)
Pain Monitor/Discrimination
Deception Task
Theory of Mind Task
Baserate
0 0.5
P(Domain|Activation)
Cognition.Memory.Working
Cognition.Social Cognition
0 0.01
P(Paradigm|Activation)
Theory of Mind Task
0 0.01

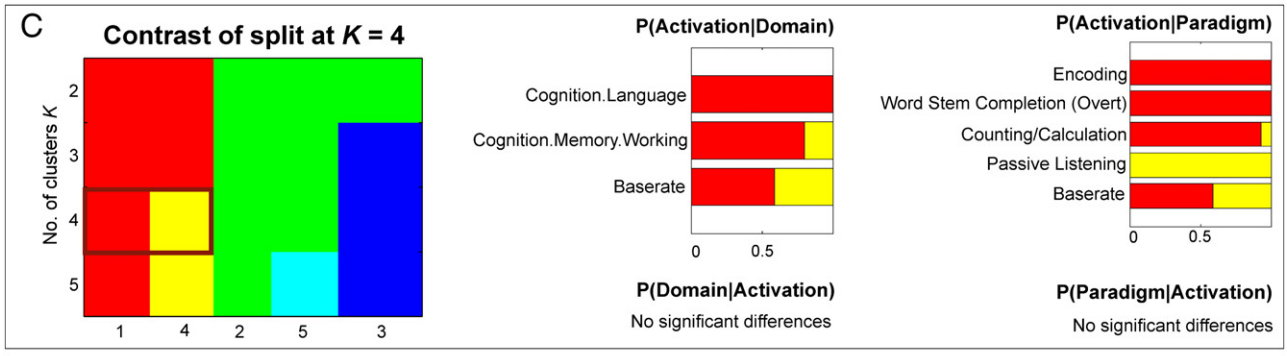
C
Contrast of split at K = 4
No. of clusters K
2
3
4
5
1 4 2 5 3
P(Activation|Domain)
Cognition.Language
Cognition.Memory.Working
Baserate
0 0.5
P(Activation|Paradigm)
Encoding
Word Stem Completion (Overt)
Counting/Calculation
Passive Listening
Baserate
0 0.5
P(Domain|Activation)
No significant differences
P(Paradigm|Activation)
No significant differences

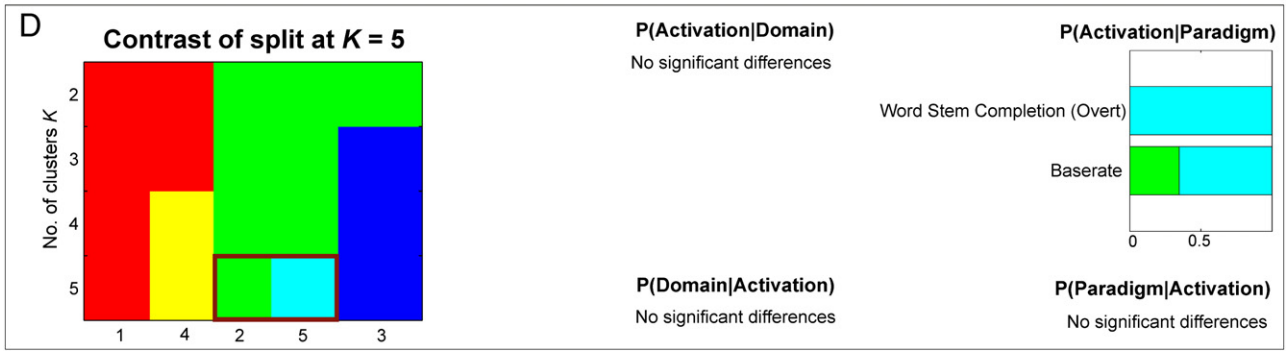
D
Contrast of split at K = 5
No. of clusters K
2
3
4
5
1 4 2 5 3
P(Activation|Domain)
No significant differences
P(Activation|Paradigm)
Word Stem Completion (Overt)
Baserate
0 0.5
P(Domain|Activation)
No significant differences
P(Paradigm|Activation)
No significant differences

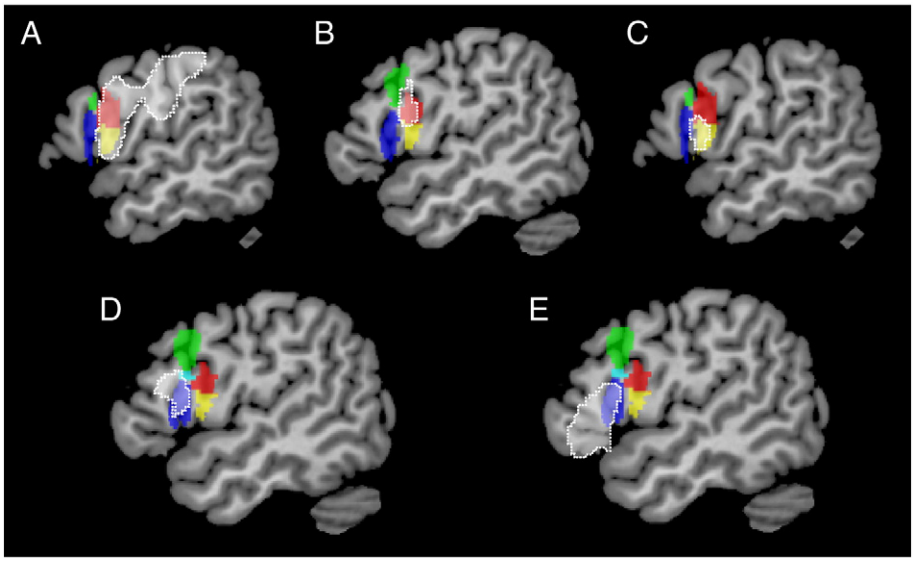

Fig. 9. External validation of functional cluster characterization. A) Activation associated with encoding and retrieval of action sequences (Kellermann et al., 2012), B) phonological word generation (Heim et al., 2008), C) action imitation (Caspers et al., 2010), D) search for meaning in degraded speech (Clos et al., 2012) and E) social evaluation of faces (Bzdok et al., 2012b) superimposed in white on the CBP-derived clusters.

left-sided MTG, amygdala and hippocampus. Firstly, the left MTG has been identified as a key region for semantic processing and meaning extraction (Binder et al., 2009; Price, 2010). Furthermore, the amygdala is not only involved in attribution of social meaning to stimuli (Heberlein and Adolphs, 2004) but also in the recognition of meaningful patterns in degraded images unrelated to emotion or social aspects (Ludmer et al., 2011). Finally, the hippocampus might be involved in the retrieval of meaningful semantic concepts and in the comparison with previously encoded semantic information (Burianova and Grady, 2007; Manns et al., 2003). Thus, we propose that the anterior-ventral cluster 3 is specifically involved in meaning extraction from sensory information and semantic processing relevant for both language comprehension and social interactions.

Finally, cluster 5 was located in the region of the inferior frontal junction (IFJ; Brass et al., 2005; Derrfuss et al., 2005; Derrfuss et al., 2009) and might correspond to two recently described areas ifj1 and ifj2 identified at the junction of the inferior frontal and the precentral sulcus by the receptor-architectonic study of Amunts et al. (2010). Cluster 5 was differentiated from cluster 2 by its higher activation probability in overt word stem completion. However, the functional inference also revealed significant association with task switching and stroop tasks that was not observed for cluster 2, nor for any other cluster in left area 44. Thus, cluster 5 seems to be particularly associated with task switching, attention, cognitive control and detection of behaviorally relevant events, matching previous functional concepts of the left IFJ (e.g. Brass et al., 2005; Derrfuss et al., 2005; Levy and Wagner, 2011). This functional characterization is furthermore in agreement with the specifically co-activated network. In particular, the pre-SMA/ MCC and the right insula are involved in switching paradigms and stroop tasks (Derrfuss et al., 2005) and detection of salient stimuli (Menon and Uddin, 2010), but also intraparietal regions are known to contribute to tasks requiring cognitive control (e.g. Brass and von Cramon, 2004; Derrfuss et al., 2004; Tomita et al., 1999) and attention (Corbetta, 1998). Thus, the cluster 5 located at the IFJ seems to be a main node in the cognitive control network composed furthermore of the insula, pre-SMA/ MCC and bilateral intraparietal sulcus.

In summary, our results demonstrate that area 44 of Broca's region and its dorsal neighborhood is a heterogeneous region that can be parcellated into five subregions based on their co-activation pattern. These subregions feature distinct connectivity and functional profiles which suggest a particular role of these in phonology and overt speech (posterior-dorsal cluster), rhythmic sequencing (posterior-ventral cluster), working memory (anterior-dorsal cluster), detection of meaning (anterior-ventral cluster), and task switching/cognitive control (inferior frontal junction cluster). While these functions should be highly relevant in the context of language production and comprehension, they will obviously also be recruited by other domains including action or social cognition.

Acknowledgments

This work was supported by the National Institute of Mental Health (R01-MH074457), the Initiative and Networking Fund of the Helmholtz Association within the Helmholtz Alliance on Systems Biology (Human Brain Model SBE, MC), the BMBF (01GW0771 to KA), and the DFG (IRTG 1328 to SBE).

Conflict of interest

There is no conflict of interest.

Appendix A. Supplementary data

Supplementary data to this article can be found online at http://dx.doi.org/10.1016/j.neuroimage.2013.06.041.

References

Amunts, K., Schleicher, A., Burgel, U., Mohlberg, H., Uylings, H.B., Zilles, K., 1999. Broca's region revisited: cytoarchitecture and intersubject variability. J. Comp. Neurol. 412, 319–341.

Amunts, K., Weiss, P.H., Mohlberg, H., Pieperhoff, P., Eickhoff, S., Gurd, J.M., Marshall, J.C., Shah, N.J., Fink, G.R., Zilles, K., 2004. Analysis of neural mechanisms underlying verbal fluency in cytoarchitectonically defined stereotaxic space—the roles of Brodmann areas 44 and 45. Neuroimage 22, 42–56.

Amunts, K., Kedo, O., Kindler, M., Pieperhoff, P., Mohlberg, H., Shah, N.J., Habel, U., Schneider, F., Zilles, K., 2005. Cytoarchitectonic mapping of the human amygdala, hippocampal region and entorhinal cortex: intersubject variability and probability maps. Anat. Embryol. (Berl.) 210, 343–352.

Amunts, K., Lenzen, M., Friederici, A.D., Schleicher, A., Morosan, P., Palomero-Gallagher, N., Zilles, K., 2010. Broca's region: novel organizational principles and multiple receptor mapping. PLoS Biol. 8, e1000489.

Anwander, A., Tittgemeyer, M., von Cramon, D.Y., Friederici, A.D., Knosche, T.R., 2007. Connectivity-based parcellation of Broca's area. Cereb. Cortex 17, 816–825.

Arbib, M.A., 2005. From monkey-like action recognition to human language: an evolutionary framework for neurolinguistics. Behav. Brain Sci. 28, 105–124.
Ashburner, J., Friston, K.J., 2005. Unified segmentation. Neuroimage 26, 839–851.
Binder, J.R., Desai, R.H., 2011. The neurobiology of semantic memory. Trends Cogn. Sci. 15, 527–536.
Binder, J.R., Desai, R.H., Graves, W.W., Conant, L.L., 2009. Where is the semantic system? A critical review and meta-analysis of 120 functional neuroimaging studies. Cereb. Cortex 19, 2767–2796.
Biswal, B., Yetkin, F.Z., Haughton, V.M., Hyde, J.S., 1995. Functional connectivity in the motor cortex of resting human brain using echo-planar MRI. Magn. Reson. Med. 34, 537–541.
Bradler, S.H., Palomero-Gallagher, N., Schleicher, A., Zilles, K., Amunts, K., 2012. Receptorarchitectonic mapping of four new areas in the inferior frontal sulcus of the human brain. Poster 885, 18th Annual Meeting of the Organization of Human Brain Mapping (OHBM), Beijing, China.
Brass, M., von Cramon, D.Y., 2004. Decomposing components of task preparation with functional magnetic resonance imaging. J. Cogn. Neurosci. 16, 609–620.
Brass, M., Derrfuss, J., Forstmann, B., von Cramon, D.Y., 2005. The role of the inferior frontal junction area in cognitive control. Trends Cogn. Sci. 9, 314–316.
Brodmann, K., 1909. Vergleichende Lokalisationslehre der Grobhirnrinde in ihren Prinzipien dargestellt auf Grund des Zellenbaues. Leipzig, Barth JA.
Brown, S., Laird, A.R., Pfordresher, P.Q., Thelen, S.M., Turkeltaub, P., Liotti, M., 2009. The somatotopy of speech: phonation and articulation in the human motor cortex. Brain Cogn. 70, 31–41.
Buchsbaum, B.R., Olsen, R.K., Koch, P., Berman, K.F., 2005. Human dorsal and ventral auditory streams subserve rehearsal-based and echoic processes during verbal working memory. Neuron 48, 687–697.
Burianova, H., Grady, C.L., 2007. Common and unique neural activations in autobiographical, episodic, and semantic retrieval. J. Cogn. Neurosci. 19, 1520–1534.
Bzdok, D., Laird, A.R., Zilles, K., Fox, P.T., Eickhoff, S.B., 2012a. An investigation of the structural, connectional, and functional subspecialization in the human amygdala. Hum. Brain Mapp. http://dx.doi.org/10.1002/hbm.22138 (Advance online publication).
Bzdok, D., Langner, R., Hoffstaedter, F., Turetsky, B.I., Zilles, K., Eickhoff, S.B., 2012b. The modular neuroarchitecture of social judgments on faces. Cereb. Cortex 22, 951–961.
Caspers, S., Geyer, S., Schleicher, A., Mohlberg, H., Amunts, K., Zilles, K., 2006. The human inferior parietal cortex: cytoarchitectonic parcellation and interindividual variability. Neuroimage 33, 430–448.
Caspers, S., Zilles, K., Laird, A.R., Eickhoff, S.B., 2010. ALE meta-analysis of action observation and imitation in the human brain. Neuroimage 50, 1148–1167.
Cauda, F., Costa, T., Torta, D.M., Sacco, K., D'Agata, F., Duca, S., Geminiani, G., Fox, P.T., Vercelli, A., 2012. Meta-analytic clustering of the insular cortex: characterizing the meta-analytic connectivity of the insula when involved in active tasks. Neuroimage 62, 343–355.
Chang, S.E., Kenney, M.K., Loucks, T.M., Poletto, C.J., Ludlow, C.L., 2009. Common neural substrates support speech and non-speech vocal tract gestures. Neuroimage 47, 314–325.
Choi, H.J., Zilles, K., Mohlberg, H., Schleicher, A., Fink, G.R., Armstrong, E., Amunts, K., 2006. Cytoarchitectonic identification and probabilistic mapping of two distinct areas within the anterior ventral bank of the human intraparietal sulcus. J. Comp. Neurol. 495, 53–69.
Cieslik, E.C., Zilles, K., Caspers, S., Roski, C., Kellermann, T.S., Jakobs, O., Langner, R., Laird, A.R., Fox, P.T., Eickhoff, S.B., 2012. Is there "one" DLPFC in cognitive action control? Evidence for heterogeneity from co-activation-based parcellation. Cereb. Cortex. http://dx.doi.org/10.1093/cercor/bhs256 (Advance online publication).
Clerget, E., Winderickx, A., Fadiga, L., Olivier, E., 2009. Role of Broca's area in encoding sequential human actions: a virtual lesion study. Neuroreport 20, 1496–1499.
Clos, M., Langner, R., Meyer, M., Oechslin, M.S., Zilles, K., Eickhoff, S.B., 2012. Effects of prior information on decoding degraded speech: an fMRI study. Hum. Brain Mapp. http://dx.doi.org/10.1002/hbm.22151 (Advance online publication).
Corballis, M.C., 2009. The evolution of language. Ann. N. Y. Acad. Sci. 1156, 19–43.
Corbetta, M., 1998. Frontoparietal cortical networks for directing attention and the eye to visual locations: identical, independent, or overlapping neural systems? Proc. Natl. Acad. Sci. U. S. A. 95, 831–838.
Costafreda, S.G., Fu, C.H., Lee, L., Everitt, B., Brammer, M.J., David, A.S., 2006. A systematic review and quantitative appraisal of fMRI studies of verbal fluency: role of the left inferior frontal gyrus. Hum. Brain Mapp. 27, 799–810.
Derrfuss, J., Brass, M., von Cramon, D.Y., 2004. Cognitive control in the posterior frontolateral cortex: evidence from common activations in task coordination, interference control, and working memory. Neuroimage 23, 604–612.
Derrfuss, J., Brass, M., Neumann, J., von Cramon, D.Y., 2005. Involvement of the inferior frontal junction in cognitive control: meta-analyses of switching and Stroop studies. Hum. Brain Mapp. 25, 22–34.
Derrfuss, J., Brass, M., von Cramon, D.Y., Lohmann, G., Amunts, K., 2009. Neural activations at the junction of the inferior frontal sulcus and the inferior precentral sulcus: interindividual variability, reliability, and association with sulcal morphology. Hum. Brain Mapp. 30, 299–311.
Dove, G., 2010. On the need for embodied and dis-embodied cognition. Front. Psychol. 1, 242.
Eickhoff, S.B., Stephan, K.E., Mohlberg, H., Grefkes, C., Fink, G.R., Amunts, K., Zilles, K., 2005. A new SPM toolbox for combining probabilistic cytoarchitectonic maps and functional imaging data. Neuroimage 25, 1325–1335.
Eickhoff, S.B., Heim, S., Zilles, K., Amunts, K., 2006a. Testing anatomically specified hypotheses in functional imaging using cytoarchitectonic maps. Neuroimage 32, 570–582.
Eickhoff, S.B., Schleicher, A., Zilles, K., Amunts, K., 2006b. The human parietal operculum. I. Cytoarchitectonic mapping of subdivisions. Cereb. Cortex 16, 254–267.
Eickhoff, S.B., Heim, S., Zilles, K., Amunts, K., 2009a. A systems perspective on the effective connectivity of overt speech production. Philos. Trans. A Math. Phys. Eng. Sci. 367, 2399–2421.
Eickhoff, S.B., Laird, A.R., Grefkes, C., Wang, L.E., Zilles, K., Fox, P.T., 2009b. Coordinate-based activation likelihood estimation meta-analysis of neuroimaging data: a random-effects approach based on empirical estimates of spatial uncertainty. Hum. Brain Mapp. 30, 2907–2926.
Eickhoff, S.B., Bzdok, D., Laird, A.R., Roski, C., Caspers, S., Zilles, K., Fox, P.T., 2011. Co-activation patterns distinguish cortical modules, their connectivity and functional differentiation. Neuroimage 57, 938–949.
Eickhoff, S.B., Bzdok, D., Laird, A.R., Kurth, F., Fox, P.T., 2012. Activation likelihood estimation meta-analysis revisited. Neuroimage 59, 2349–2361.
Evans, A.C., Janke, A.L., Collins, D.L., Baillet, S., 2012. Brain templates and atlases. Neuroimage 62, 911–922.
Fazio, P., Cantagallo, A., Craighero, L., D'Ausilio, A., Roy, A.C., Pozzo, T., Calzolari, F., Granieri, E., Fadiga, L., 2009. Encoding of human action in Broca's area. Brain 132, 1980–1988.
Femyhough, C., Meins, E., 2009. Private speech and theory of mind: Evidence for developing interfunctional relations. In: Winsler, A., Fernyhough, C., Montero, I. (Eds.), Private speech, executive functioning, and the development of verbal self-regulation. Cambridge University Press, New York (NY US), pp. 95–104.
Ford, A., McGregor, K.M., Case, K., Crosson, B., White, K.D., 2010. Structural connectivity of Broca's area and medial frontal cortex. Neuroimage 52, 1230–1237.
Fox, P.T., Lancaster, J.L., 2002. Opinion: mapping context and content: the BrainMap model. Nat. Rev. Neurosci. 3, 319–321.
Fox, M.D., Raichle, M.E., 2007. Spontaneous fluctuations in brain activity observed with functional magnetic resonance imaging. Nat. Rev. Neurosci. 8, 700–711.
Friederici, A.D., 2011. The brain basis of language processing: from structure to function. Physiol. Rev. 91, 1357–1392.
Geyer, S., 2004. The microstructural border between the motor and the cognitive domain in the human cerebral cortex. Adv. Anat. Embryol. Cell Biol. 174, 1–89.
Geyer, S., Ledberg, A., Schleicher, A., Kinomura, S., Schormann, T., Burgel, U., Klingberg, T., Larsson, J., Zilles, K., Roland, P.E., 1996. Two different areas within the primary motor cortex of man. Nature 382, 805–807.
Greicius, M.D., Krasnow, B., Reiss, A.L., Menon, V., 2003. Functional connectivity in the resting brain: a network analysis of the default mode hypothesis. Proc. Natl. Acad. Sci. U.S.A. 100, 253–258.
Hagoort, P., 2005. On Broca, brain, and binding: a new framework. Trends Cogn. Sci. 9, 416–423.
Hartigan, J.A., Wong, M.A., 1979. A k-means clustering algorithm. Appl. Stat. 28, 100–108.
Heberlein, A.S., Adolphs, R., 2004. Impaired spontaneous anthropomorphizing despite intact perception and social knowledge. Proc. Natl. Acad. Sci. U.S.A. 101, 7487–7491.
Heim, S., Eickhoff, S.B., Amunts, K., 2008. Specialisation in Broca's region for semantic, phonological, and syntactic fluency? Neuroimage 40, 1362–1368.
Heiser, M., Iacoboni, M., Maeda, F., Marcus, J., Mazziotta, J.C., 2003. The essential role of Broca's area in imitation. Eur. J. Neurosci. 17, 1123–1128.
Iacoboni, M., Woods, R.P., Brass, M., Bekkering, H., Mazziotta, J.C., Rizzolatti, G., 1999. Cortical mechanisms of human imitation. Science 286, 2526–2528.
Jakobs, O., Langner, R., Caspers, S., Roski, C., Cieslik, E.C., Zilles, K., Laird, A.R., Fox, P.T., Eickhoff, S.B., 2012. Across-study and within-subject functional connectivity of a right temporo-parietal junction subregion involved in stimulus-context integration. Neuroimage 60, 2389–2398.
Johansen-Berg, H., Behrens, T.E., Robson, M.D., Drobnjak, I., Rushworth, M.F., Brady, J.M., Smith, S.M., Higham, D.J., Matthews, P.M., 2004. Changes in connectivity profiles define functionally distinct regions in human medial frontal cortex. Proc. Natl. Acad. Sci. U.S.A. 101, 13335–13340.
Kaan, E., Swaab, T.Y., 2002. The brain circuitry of syntactic comprehension. Trends Cogn. Sci. 6, 350–356.
Kahnt, T., Chang, L.J., Park, S.Q., Heinzle, J., Haynes, J.D., 2012. Connectivity-based parcellation of the human orbitofrontal cortex. J. Neurosci. 32, 6240–6250.
Kellermann, T.S., Sternkopf, M.A., Schneider, F., Habel, U., Turetsky, B.I., Zilles, K., Eickhoff, S.B., 2012. Modulating the processing of emotional stimuli by cognitive demand. Soc. Cogn. Affect. Neurosci. 7, 263–273.
Kelly, C., Uddin, L.Q., Shehzad, Z., Margulies, D.S., Castellanos, F.X., Milham, M.P., Petrides, M., 2010. Broca's region: linking human brain functional connectivity data and non-human primate tracing anatomy studies. Eur. J. Neurosci. 32, 383–398.
Klein, J.C., Behrens, T.E., Robson, M.D., Mackay, C.E., Higham, D.J., Johansen-Berg, H., 2007. Connectivity-based parcellation of human cortex using diffusion MRI: establishing reproducibility, validity and observer independence in BA 44/45 and SMA/pre-SMA. Neuroimage 34, 204–211.
Koelsch, S., 2011. Toward a neural basis of music perception — a review and updated model. Front. Psychol. 2, 110.
Koelsch, S., Gunter, T.C., Cramon, D.Y., Zysset, S., Lohmann, G., Friederici, A.D., 2002. Bach speaks: a cortical "language-network" serves the processing of music. Neuroimage 17, 956–966.
Laird, A.R., Lancaster, J.L., Fox, P.T., 2005. BrainMap: the social evolution of a human brain mapping database. Neuroinformatics 3, 65–78.
Laird, A.R., Eickhoff, S.B., Kurth, F., Fox, P.M., Uecker, A.M., Turner, J.A., Robinson, J.L., Lancaster, J.L., Fox, P.T., 2009a. ALE meta-analysis workflows via the Brainmap database: progress towards a probabilistic functional brain atlas. Front. Neuroinform. 3, 23.
Laird, A.R., Eickhoff, S.B., Li, K., Robin, D.A., Glahn, D.C., Fox, P.T., 2009b. Investigating the functional heterogeneity of the default mode network using coordinate-based meta-analytic modeling. J. Neurosci. 29, 14496–14505.
Laird, A.R., Eickhoff, S.B., Fox, P.M., Uecker, A.M., Ray, K.L., Saenz Jr., J.J., McKay, D.R., Bzdok, D., Laird, R.W., Robinson, J.L., Turner, J.A., Turkeltaub, P.E., Lancaster, J.L.,

Fox, P.T., 2011. The BrainMap strategy for standardization, sharing, and meta-analysis of neuroimaging data. BMC Res. Notes 4, 349.
Levy, B.J., Wagner, A.D., 2011. Cognitive control and right ventrolateral prefrontal cortex: reflexive reorienting, motor inhibition, and action updating. Ann. N. Y. Acad. Sci. 1224, 40–62.
Ludmer, R., Dudai, Y., Rubin, N., 2011. Uncovering camouflage: amygdala activation predicts long-term memory of induced perceptual insight. Neuron 69, 1002–1014.
Maess, B., Koelsch, S., Gunter, T.C., Friederici, A.D., 2001. Musical syntax is processed in Broca's area: an MEG study. Nat. Neurosci. 4, 540–545.
Makuuchi, M., Bahlmann, J., Anwander, A., Friederici, A.D., 2009. Segregating the core computational faculty of human language from working memory. Proc. Natl. Acad. Sci. U. S. A. 106, 8362–8367.
Manns, J.R., Hopkins, R.O., Squire, L.R., 2003. Semantic memory and the human hippocampus. Neuron 38, 127–133.
Meila, M., 2007. Comparing clusterings — an information based distance. J. Multivar. Anal. 98, 873–895.
Menon, V., Uddin, L.Q., 2010. Saliency, switching, attention and control: a network model of insula function. Brain Struct. Funct. 214, 655–667.
Nichols, T., Brett, M., Andersson, J., Wager, T., Poline, J.B., 2005. Valid conjunction inference with the minimum statistic. Neuroimage 25, 653–660.
Nickl-Jockschat, T., Habel, U., Michel, T.M., Manning, J., Laird, A.R., Fox, P.T., Schneider, F., Eickhoff, S.B., 2012. Brain structure anomalies in autism spectrum disorder — a meta-analysis of VBM studies using anatomic likelihood estimation. Hum. Brain Mapp. 33, 1470–1489.
Nooner, K.B., Colcombe, S.J., Tobe, R.H., Mennes, M., Benedict, M.M., Moreno, A.L., Panek, L.J., Brown, S., Zavitz, S.T., Li, Q., Sikka, S., Gutman, D., Bangaru, S., Schlachter, R.T., Kamiel, S.M., Anwar, A.R., Hinz, C.M., Kaplan, M.S., Rachlin, A.B., Adelsberg, S., Cheung, B., Khanuja, R., Yan, C., Craddock, C.C., Calhoun, V., Courtney, W., King, M., Wood, D., Cox, C.L., Kelly, A.M., Di, M.A., Petkova, E., Reiss, P.T., Duan, N., Thomsen, D., Biswal, B., Coffey, B., Hoptman, M.J., Javitt, D.C., Pomara, N., Sidtis, J.J., Koplewicz, H.S., Castellanos, F.X., Leventhal, B.L., Milham, M.P., 2012. The NKI-Rockland sample: a model for accelerating the pace of discovery science in psychiatry. Front. Neurosci. 6, 152.
Ochsner, K.N., Knierim, K., Ludlow, D.H., Hanelin, J., Ramachandran, T., Glover, G., Mackey, S.C., 2004. Reflecting upon feelings: an fMRI study of neural systems supporting the attribution of emotion to self and other. J. Cogn. Neurosci. 16, 1746–1772.
Platel, H., Price, C., Baron, J.C., Wise, R., Lambert, J., Frackowiak, R.S., Lechevalier, B., Eustache, F., 1997. The structural components of music perception. A functional anatomical study. Brain 120 (Pt 2), 229–243.
Price, C.J., 2010. The anatomy of language: a review of 100 fMRI studies published in 2009. Ann. N. Y. Acad. Sci. 1191, 62–88.
Reetz, K., Dogan, I., Rolfs, A., Binkofski, F., Schulz, J.B., Laird, A.R., Fox, P.T., Eickhoff, S.B., 2012. Investigating function and connectivity of morphometric findings — exemplified on cerebellar atrophy in spinocerebellar ataxia 17 (SCA17). Neuroimage 62, 1354–1366.
Rizzolatti, G., Arbib, M.A., 1998. Language within our grasp. Trends Neurosci. 21, 188–194.
Rizzolatti, G., Craighero, L., 2004. The mirror-neuron system. Annu. Rev. Neurosci. 27, 169–192.
Rogalsky, C., Hickok, G., 2011. The role of Broca's area in sentence comprehension. J. Cogn. Neurosci. 23, 1664–1680.
Rottschy, C., Langner, R., Dogan, I., Reetz, K., Laird, A.R., Schulz, J.B., Fox, P.T., Eickhoff, S.B., 2012. Modelling neural correlates of working memory: a coordinate-based meta-analysis. Neuroimage 60, 830–846.
Scheperjans, F., Hermann, K., Eickhoff, S.B., Amunts, K., Schleicher, A., Zilles, K., 2008. Observer-independent cytoarchitectonic mapping of the human superior parietal cortex. Cereb. Cortex 18, 846–867.
Smith, E.E., Jonides, J., 1999. Storage and executive processes in the frontal lobes. Science 283, 1657–1661.
Sommer, I.E., Clos, M., Meijering, A.L., Diederen, K.M., Eickhoff, S.B., 2012. Resting state functional connectivity in patients with chronic hallucinations. PLoS One 7, e43516.
Stevens, M.C., Kiehl, K.A., Pearlson, G., Calhoun, V.D., 2007. Functional neural circuits for mental timekeeping. Hum. Brain Mapp. 28, 394–408.
Tomita, H., Ohbayashi, M., Nakahara, K., Hasegawa, I., Miyashita, Y., 1999. Top-down signal from prefrontal cortex in executive control of memory retrieval. Nature 401, 699–703.
Turkeltaub, P.E., Eden, G.F., Jones, K.M., Zeffiro, T.A., 2002. Meta-analysis of the functional neuroanatomy of single-word reading: method and validation. Neuroimage 16, 765–780.
Turkeltaub, P.E., Eickhoff, S.B., Laird, A.R., Fox, M., Wiener, M., Fox, P., 2012. Minimizing within-experiment and within-group effects in Activation Likelihood Estimation meta-analyses. Hum. Brain Mapp. 33, 1–13.
Walters, N.B., Eickhoff, S.B., Schleicher, A., Zilles, K., Amunts, K., Egan, G.F., Watson, J.D., 2007. Observer-independent analysis of high-resolution MR images of the human cerebral cortex: in vivo delineation of cortical areas. Hum. Brain Mapp. 28, 1–8.
Wang, J., Conder, J.A., Blitzer, D.N., Shinkareva, S.V., 2010. Neural representation of abstract and concrete concepts: a meta-analysis of neuroimaging studies. Hum. Brain Mapp. 31, 1459–1468.
Weissenbacher, A., Kasess, C., Gerstl, F., Lanzenberger, R., Moser, E., Windischberger, C., 2009. Correlations and anticorrelations in resting-state functional connectivity MRI: a quantitative comparison of preprocessing strategies. Neuroimage 47, 1408–1416.
Zahn, R., Moll, J., Krueger, F., Huey, E.D., Garrido, G., Grafman, J., 2007. Social concepts are represented in the superior anterior temporal cortex. Proc. Natl. Acad. Sci. U.S.A. 104, 6430–6435.
Zhang, S., Li, C.S., 2012. Functional connectivity mapping of the human precuneus by resting state fMRI. Neuroimage 59, 3548–3562.
zu Eulenburg, P., Caspers, S., Roski, C., Eickhoff, S.B., 2012. Meta-analytical definition and functional connectivity of the human vestibular cortex. Neuroimage 60, 162–169.